THESIS FOR THE DEGREE OF DOCTOR OF PHILOSOPHY

On the mechanics of pulp fibre networks

A combined numerical, theoretical and experimental study

PER BERGSTRÖM

Department of Mechanics and Maritime Sciences

CHALMERS UNIVERSITY OF TECHNOLOGY

Gothenburg, Sweden 2023

On the mechanics of pulp fibre networks
A combined numerical, theoretical and experimental study
PER BERGSTRÖM
ISBN 978-91-7905-933-0

Doktorsavhandlingar vid Chalmers tekniska högskola
Ny serie nr 5399
ISSN 0346-718X

Department of Mechanics and Maritime Sciences
Chalmers University of Technology
SE-412 96 Gothenburg
Sweden
Telephone + 46 (0)31-772 1000

Chalmers digitaltryck
Gothenburg, Sweden 2023

On the mechanics of pulp fibre networks

PER BERGSTRÖM
Department of Mechanics and Maritime Sciences
Division of Fluid Dynamics
Chalmers University of Technology

Abstract

This work explores mechanics of fibre networks, especially for pulp fibre networks commonly found in hygiene products, such as baby diapers, incontinence and feminine care products, bathroom tissue and kitchen towels. Given that the main functionalities of these products are directly dependent on network configuration, designing these complex network structures for better performance, better utilisation of materials and less resources used requires in-depth knowledge and understanding of the structure and properties on the fibre level. The current work combines experimental, theoretical, and numerical results using the Discrete Element Method (DEM) to further this in-depth understanding of network deformation. The investigation starts with focusing on the effect of compression on network deformation, showing how deformation of the constituent fibres are dominated by bending of fibres at low solid volume fraction while at higher solid volume fraction transitioning to being dominated by fibre-fibre contact deformation. This is followed by showing the relationship between network solid volume fraction and tensile strength and stiffness. We continue by shifting the focus to permanent network deformation. The effect of fibre-fibre adhesion and fibre plastic contact deformation on permanent network deformation due to compression is investigated. Results show a synergetic effect of combining the two phenomena resulting in a significant increase in permanent deformation. Finally, we explain the dominating physics behind deformation due to the network transitioning from a dry to a wet state showing how the network reverts to a state of maximum unforced packing. The novel findings in this work further elucidates the mechanisms behind deformation of fibre networks, in particular for pulp fibre networks, and in consequence the functionality of products consisting of such networks. This knowledge provides insights that can be translated into improved performance, more sustainable resource use as well as optimization of the manufacturing process for a wide range of hygiene products.

Keywords: Fibre networks, mechanics, pulp fibres, Discrete element method.

Acknowledgements

I would like to gratefully thank my supervisor Srdjan Sasic for his excellent supervision and support for me in exploring this complex and fascinating subject. I have found our collaborative efforts challenging, inspiring and always truly enjoyable. I would also like to thank my co-supervisor Henrik Ström for his valuable input and assistance throughout the project. I have learnt so much from you both and hope we can continue to collaborate in the future. A special thank you to Charlotta Hanson, my dear colleague and friend, for her insightful assistance and unwavering support. You were always there for me and I am deeply grateful.

I would like to thank the department of Mechanics and Maritime Sciences and division of Fluid Dynamics for allowing me to pursue my PhD with you, I will always cherish my time spent with you, full of interesting discussions and wonderful co-workers.

I would also like to thank my employer Essity for enabling my research and all my amazing colleagues for inspiring me, supporting me and for utilizing my results.

For the first part of my work, encompassing Paper I and Paper II in this thesis and previously covered in my licentiate, I would like to appreciatively acknowledge the Mid Sweden University, my former supervisor Tetsu Uesaka and colleague Shakhawath Hossain.

I would finally like to thank my beloved family – Sofia, Märtha and Abbe – without your love and support none of this would have been possible.

List of publications

This thesis is based on the work in the following papers:

I. Hossain, M. S., Bergström, P., & Uesaka, T. (2018). Uniaxial compression of three-dimensional entangled fibre networks: impacts of contact interactions. *Modelling and Simulation in Materials Science and Engineering*, 27(1), 015006.

II. Bergström, P., Hossain, S., & Uesaka, T. (2019). Scaling behaviour of strength of 3D-, semi-flexible-, cross-linked fibre network. *International Journal of Solids and Structures*, 166, 68-74.

III. Bergström, P., Hanson, C., Ström, H., & Sasic, S. (2022). Uniaxial compression of fibre networks–the synergetic effect of adhesion and elastoplasticity on non-reversible deformation. *Powder Technology*, 395, 301-313.

IV. Bergström, P., Hanson, C., Ström, H., & Sasic, S. (2023). The dry-to-wet transition of fiber networks—Return to mechanical stability. *AIChE Journal*, e18148.

Additional relevant publications:

V. P. Bergström, H. Ström, C. Hansson and S. Sasic, Mechanical and fluid-transport properties of fiber networks – fundamental differences between dry and wet networks, *11th International Conference on Multiphase Flow* (ICMF2023), Kobe, Japan, 2023.

VI. Röding, M., Schuster, E., Logg, K., Lundman, M., Bergström, P., Hanson, C., ... & Lorén, N. (2016). Computational high-throughput screening of fluid permeability in heterogeneous fiber materials. *Soft Matter*, 12(29), 6293-6299.

VII. Townsend, P., Larsson, E., Karlson, T., Hall, S. A., Lundman, M., Bergström, P., ... & Röding, M. (2021). Stochastic modelling of 3D fiber structures imaged with X-ray microtomography. *Computational Materials Science*, 194, 110433.

VIII. Hossain, S., Bergström, P., Sarangi, S., & Uesaka, T. (2017). Computational design of fibre network by discrete element method. *The 16th Pulp and Paper Fundamental Research Symposium*, Oxford, UK, 3-8 September 2017.

IX. Hossain, M. S., Bergström, P., & Uesaka, T. (2016). A Particle-based Model to Investigate the Mechanics of Soft Fibre Network. *World Congress of Computational Mechanics and ECCOMAS* 2016, Crete, Greece.

X. Hossain, S., Bergström, P., & Uesaka, T. (2017). Non-Affine Deformation Of Soft Fibre Network. *Svenska Mekanikdagar*, Uppsala, Sweden, 12-13 juni 2017 (p. 46).

Contents

Extended Summary

1. Introduction

This thesis concerns modelling of mechanics of fibre networks, especially for low density pulp fibre networks commonly found in hygiene products, such as baby diapers, incontinence and feminine care products, bathroom tissue and kitchen towels. These common household products are used on a regular basis by billions of people around the world to handle their everyday life. The performance of these products helps users with widely varying aspects of life, from cleaning up spilled milk and hand hygiene to the handling of menstruation and incontinence. For this range of products, some of the most important performance properties are directly related to the mechanics of the respective fibre networks. Softness, pliability and structural integrity are crucial product properties. Additionally, since the primary functionality of the products is the absorption of liquids, fluid transport properties of the network are also primary performance properties. Due to the nature of this type of materials, connected fibres in a matrix of void, an important characteristic of networks for both mechanical properties and fluid transport properties is the relationship between the fibre volume and the void volume. In this work this relationship is characterized by the solid volume fraction (SVF), defined as the ratio of fibre volume per total volume. Properties like permeability and capillary pressure, as well as network strength and stiffness are strongly dependent on the solid volume fraction of the network and hence dependent on network deformation. This influence is often used in industry in attempts to tailor materials with specific mechanical and fluid transport properties. The geometry of the selected fibres, inter-fibre bonding and the degree of deformation is used to manufacture materials with specific function. However, due to the presence of, in many cases, extreme softness or deformability of this type of networks, even the smallest stress on the networks during end-use can have a significant impact on the solid volume fraction of the material and, consequently, on both the mechanical behaviour and the fluid transport properties of the product.

The importance of mechanical properties and deformation, both in production and in end-use, poses constant challenges for product designers in designing network structures for improved product performance, better use of materials, and lower costs. These challenges demand ever-increasing need for in-depth knowledge and understanding of the network and properties on the fibre level. From an application point of view, a key question is understanding the dependence of mechanical properties and deformation of the network on individual fibres and their properties. The reason for this is that a typical design question is not about constitutive parameters but rather about the effects on end-use performance of fibre properties, such as fibre-shape, -length and -stiffness, together with the effects of specific steps of the manufacturing process (for example compression). This leads to a great importance of understanding network deformation and its relation to the properties of the constituent fibres when designing networks for optimal product function.

When using a modelling approach to create this in-depth knowledge and understanding, the choice of the models is crucial for the end result, both for attaining a representative network structure and understanding network deformation. In this study we choose to model our networks as a discrete system in three dimensions (3D) and pay special attention to fibre–fibre interactions in order to evaluate network deformations. We have used a particle-based method termed the Discrete Element Method (DEM), which is a robust and intuitive method well suited for handling important features of network deformation such as large deformation, relative translation/rotation of components and the important emergence/breakage of contacts between components which characterizes this type of structures. Using DEM, we have developed a numerical framework and used it for in-depth

understanding of the relationship between network deformation and properties of the constituent fibres in four cases important for end-use properties. The selected cases are: i) the effect of compression on network deformation, ii) the relationship between network solid volume fraction and tensile strength and stiffness, iii) the effect of fibre-fibre adhesion and plastic contact deformation on permanent network deformation due to compression and, iv) the effect of spontaneous network deformation due to the network transitioning from a dry to a wet state. In the following, we will look at how these subjects have been discussed in the literature.

2. Background

A fibre network is a commonly seen structure in industrial materials, not only hygiene products and paper but also nonwovens, filters and isolation materials. It can also be related to networks formed in agricultural processes such as packed hay or industrial processes involving the stacking or packing of elongated particles. Fibre networks are also prominently occurring in biological materials such as collagen fibre networks and in the cytoskeleton of eucaryotic cells. These networks are often used industrially and encountered in the biological world for their combination of mechanical properties in relation to weight, as well as their fluid transport properties due to the inherent permeable nature of these materials.

Fibre networks can be categorized into a number of subclasses, such as bonded or unbonded networks, rigid, flexible or semi-flexible, and isotropic or anisotropic.[1] In this classification bonded networks are seen as networks where fibres are mechanically attached to each other at fibre-fibre contact points, which prohibits the relative sliding and detachment of fibres in these contacts. This leads to a relatively more mechanically stable structure and tending to a more elastic behaviour of the material. Materials often characterized in this class include several biological networks such as those of collagen or cytoskeleton of eucaryotic cells. It also includes industrial materials like paper and nonwoven. The counterpart to bonded networks are unbonded fibre networks where fibres are unrestricted from detaching and from relative sliding in contact points aside from the impact of fibre-fibre friction, known as fibre rearrangement. The structural integrity in this case is very much related to the entanglement of the constituent fibres which has led to this class of network sometimes being referred to as entangled networks. Unbonded fibre networks, as opposed to bonded networks, tend to lead to networks with relatively less mechanical stability and often prone to non-elastic or non-reversible deformation due to relative sliding of the constituent fibres. Materials often characterized in this class include pulp fibre networks in hygiene products and stacks of agricultural or industrial products. In between these two classes there exist networks expressing behaviour of both bonded and unbonded networks depending on circumstances. This includes weakly bonded networks (bonded networks where bonds easily break) or adhesive networks, where attractive forces between fibres form bonds at fibre-fibre contact points that can detach and re-attach during deformation. The pulp fibre networks that we are primarily interested in in this work can be classified as semi-flexible, anisotropic networks ranging from unbonded to weakly or adhesively bonded.

Modelling compressibility of fibre networks has a long history, originating in the textile area. Here, compressibility is defined as the uniaxial compression response of fibre network in the thickness direction (z-direction) in relation to solid volume fraction or the closely related network density, with different terminology being used in different communities. The pioneering work of compression modelling is the semi-empirical model developed by van Wyk[2] where he proposed the expression for pressure, P, as a function of solid volume fraction ϕ:

$$P \propto \left(\left(\frac{\phi}{\phi_0}\right)^n - 1\right) \qquad \textit{(Eq. 1)}$$

where ϕ_0 is the unloaded solid volume fraction. The exponent, *n*, is describing the development of pressure and was found by van Wyk to be equal to 3 for originally isotropic networks. The work was followed up by several researchers using statistical geometry modelling to address the issues such as the effect of anisotropy, the development of fibre-fibre contacts and the steric hindrance effect on fibre-fibre contacts.[3-7] Notably it was shown by Toll and Månson that the exponent *n* equalled to 5

for networks with planar fibre orientation, in contrast to the value of 3 obtained by van Wyk for isotropic networks.[6] For the development of fibre-fibre contacts Komori and Makishima developed what is commonly referred to as a random contact equation to describe the relationship between solid volume fraction and number of fibre-fibre contacts.[3] It was shown that the change in the number of contacts is directly proportional to the change in the solid volume fraction. Further extension of the work includes Toll deriving an equation for the number of fibre-fibre contacts accounting for effects from fibre orientation.[5]

$$N_c = \frac{8}{\pi}\phi r f + 4\phi(g+1) \qquad \textit{(Eq. 2)}$$

where N_c is the average number of fibre-fibre contacts per fibre, defined as the average number of contacts a fibre experiences (not to be confused with the total number of fibre-fibre contacts in a network divided by the total number of fibres). *r* is the fibre aspect ratio. *f* and *g* are scalars dependent on the fibre orientation. In the case of 3D random orientation, *f* and *g* take the values $\pi/4$ and 1/2, respectively. For 2D random orientation $f = g = 2/\pi$ and for aligned fibers, $f = 0$, $g = 1$. For non-aligned slender fibres with $r \gg 1$ this can be reduced to:[5]

$$N_c = \frac{8}{\pi}\phi r f \qquad \textit{(Eq. 3)}$$

Other statistical geometry considerations regarding the nature of random fibre networks related to the *maximum unforced packing* of fibres. The latter is defined as the volume fraction at which a given network cannot be further compressed without deformation or interpenetration of rods. Evans and Gibson suggested that this occurs when the average fibre is restricted from any translational or rotational motion due to contacts from neighbouring fibres.[8] By using the *caging number,* defined as the average minimum number of randomly placed fibre-fibre contacts on a single fibre that immobilize all its translations and rotations, this allows for estimating the maximum unforced packing of a network using a random contact equation with N_c equal to the caging number. Using Toll's formulation of the random contact equation this leads to the following equation:

$$\phi_{max} = \frac{\pi}{8}\frac{\gamma}{rf} \qquad \textit{(Eq. 4)}$$

where ϕ_{max} is the solid volume fraction at maximum unforced packing and γ is the caging number.

Following the achievements using statistical modelling further studies on mechanics of fibre networks focused on overcoming the shortcomings of the statistical approach. While proving very successful in characterizing networks, the models developed require some crucial assumptions, such as affine deformation of a fibre beam segment, leading to friction and sliding between fibres not being explicitly considered. The models also assume bending deformation of fibres as the only fibre deformation mode, ignoring fibre shear, twist, stretch and deformation of fibre in the transverse direction. This led to researchers turning to numerical studies of fibre networks mechanics primarily using discrete element (DEM) or bead-spring models to capture fibre deformation and also to account for fibre-fibre rearrangement.[9-17] The latter is an important aspect, especially in non-bonded networks, as it significantly impacts both the overall response and the non-reversible deformation of these soft materials. A study by Rodney et al. confirmed that the simulated stresses using this class of models followed the dependence on the solid volume fraction (SVF) predicted by van Wyk, a power function with an exponent of 3, and that the number of fibre-fibre contacts increased linearly with SVF.[9] The numerical models were shown to account for fibre rearrangement, in some cases leading to non-reversible deformation due to compression.[10,11] The fibre deformation mechanism has also been further clarified, where Subramanian & Picu showed that for triaxial compression of isotropic networks in the initial stage of compression fibres deform mainly in the bending mode, whereas in

the high-density range the fibre axial deformation mode starts to dominate.[10] This type of transition behaviour in terms of a dominating deformation mode had already been shown for tensile deformation of bonded networks, from the work of Head et al., where the deformation mode transitions between bending and axial deformation depending on the network solid volume fraction and deformation.[18]

It is noteworthy that there are studies that specifically focused on using numerical methods for further capturing the effects of fibre deformation and contact mechanics. Notably, Guo et al. simulated uniaxial compression of fibre assemblies by studying compression force development and hysteresis in the loading-unloading cycle for different contact force models and plastic deformation of fibres.[19] It was found that the elastic fibre bending model overpredicted the loads compared to an elasto-plastic model in the low solid volume fraction range and that the elastic fibre-fibre contact model overpredicted the loads compared to an elasto-plastic model in the high solid volume fraction range. Using adhesive contact models, Negi and Picu studied response of non-bonded planar fibre networks stabilised by fibre-fibre adhesion due tensile loading.[15] The same authors studied mechanical behaviour of bonded fibre networks with inter-fibre adhesion in uniaxial compression using a 2D model. The results in compression for small strains showed an initial linear elastic regime followed by strain localization.[16]

Numerical simulations were also used to investigate the networks in relation to stability onset and maximum unforced packing. For fibres with a high aspect ratio, Wouterse et al. found the caging number of fibres to be 9 by using Linear Complementarity Problem calculations.[20] The same authors compared their findings to mechanical contraction simulations using Molecular Dynamics simulations for random packing of thin rods of constant length to determine the stability onset, defined as the limiting solid volume fraction upon which further contraction leads to a non-vanishing pressure. The authors found the average number of fibre-fibre contacts to be dependent on the aspect ratio for fibres with a low aspect ratio, while having a constant value around 7.5 for fibres with an aspect ratio above 40.[20]

Overall, these findings paint the picture of non-bonded, semi-flexible fibre networks, the class to which pulp fibre networks is often attributed, as being a class of materials with a wide range of regimes and with very varying responses to stresses. Networks are characterized by the strong influence of the solid volume fraction on macroscopic properties like mechanical properties and fluid transport properties in combination with an extreme deformability of the material. This leads to that slight changes in stress, historic stress or changes in fibre-fibre interactions can lead to major changes in macroscopic material properties and changes in dominating factors for network deformation. This results in a material with ever-changing properties. It is, therefore, crucial to understand changes in the solid volume fraction and the dominating factors for network deformation under the present circumstances in order to understand the macroscopic behaviour of the material.

3. Objectives

The overall goal of this thesis has been to develop fundamental understanding of the complex mechanics of non-bonded, anisotropic fibre networks such as the pulp fibre networks commonly found in hygiene products. The focus has been placed in a few selected areas not previously covered in literature, but with great relevance for the development of products consisting of pulp fibre networks.

- First, we focus on uniaxial compression of anisotropic as opposed to isotropic fibre networks to further understand the relationship between network deformation and deformation of the constituent fibres for this type of networks by investigating the dominating fibre deformation mode for different degrees of compression.
- Second, we focus on deformation due to tensile stress and study the scaling of elastic modulus with network solid volume fraction and the scaling of strength and strain-to-failure with solid volume fraction and fibre-fibre bond strength in anisotropic networks of low solid volume fraction.
- Third, we focus on non-reversible deformation due to uniaxial compression and investigate the contribution of fibre rearrangement, fibre-fibre adhesion and elasto-plastic contact deformation of fibres on the subsequent change in unloaded solid volume fraction of networks.
- Finally, we study the change in the solid volume fraction in pulp fibre networks due to transitioning from a dry to a wet state. In this work we aim to characterize the state to which the network transitions and identify the main mechanisms driving the change in the network solid volume fraction.

4. Methodology

In order to achieve the objectives of this work we combine experimental, numerical and theoretical approaches, with all three perspectives contributing to create a complete picture.

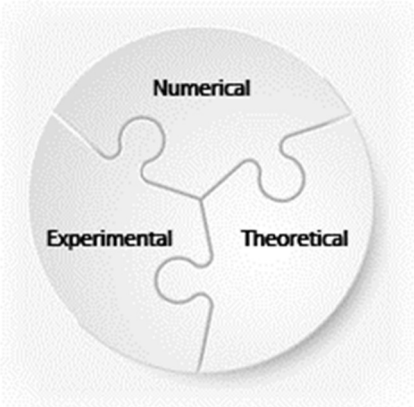

Fig 1: Illustration of combining experimental, numerical and theoretical approache to create a complete picture.

The focus of experimental procedures has been, given the importance of the network solid volume fraction on network response to deformation, to quantify and characterize changes of this parameter. For numerical results, a framework has been developed for seamlessly generating and testing fibre networks by using the Discrete Element Method (DEM). DEM is commonly used to model and analyse packing, mixing and dynamics of granular materials on a particle-level in a wide range of applications such as mining, agriculture and soil science.[21-25] The main goal in this work has been to obtain information on a fibre-level unattainable by experimental methods, such as fibre deformation and quantification of fibre-fibre contacts, as well as the ability to fully control the physics involved in order to independently study the impact of different phenomena. In addition, we complement our experimental and numerical work with theoretical explanations and make use of the existing fibre network theory from literature. This includes utilizing theory for network configuration and the relationship between the solid volume fraction and the number of fibre-fibre contacts from statistical geometry modelling, as well as using the theory for fibre-level phenomena such as caging of fibres.[5,20]

4.1 Experimental methodology

Experimental procedures were performed in all the papers included in this thesis, with the exception of Paper II where experimental results from literature were used. The purpose of these measurements was to characterize network deformation and serve as a basis for understanding the underlying physics.

Due to the objectives of this work, much of the experimental methods revolves around network solid volume fraction and changes to network solid volume fraction of pulp fibre networks under various conditions. Samples used for measurement consisted of networks of the type often found in personal hygiene products, consisting of air-laid Southern Pine pulp fibres. The process of creating the network involves separated fibres transported in air being deposited on a perforated plate resulting in a low-solid volume fraction anisotropic network.

The solid volume fraction of the sample is calculated as $\phi = \left(m/\rho_f\right)/(A \cdot h)$, where ϕ is the network solid volume fraction, m is the sample mass, ρ_f is the fibre density, *A* is the area under load and *h* is the thickness (height) of the sample. Thickness was measured either continuously or under

constant static load. Continuous measurements under increasing or decreasing load were performed using an Instron tensile testing machine equipped for compression measurements. Measuring thickness under constant static load was performed using electronic thickness gauge (Fig 2).

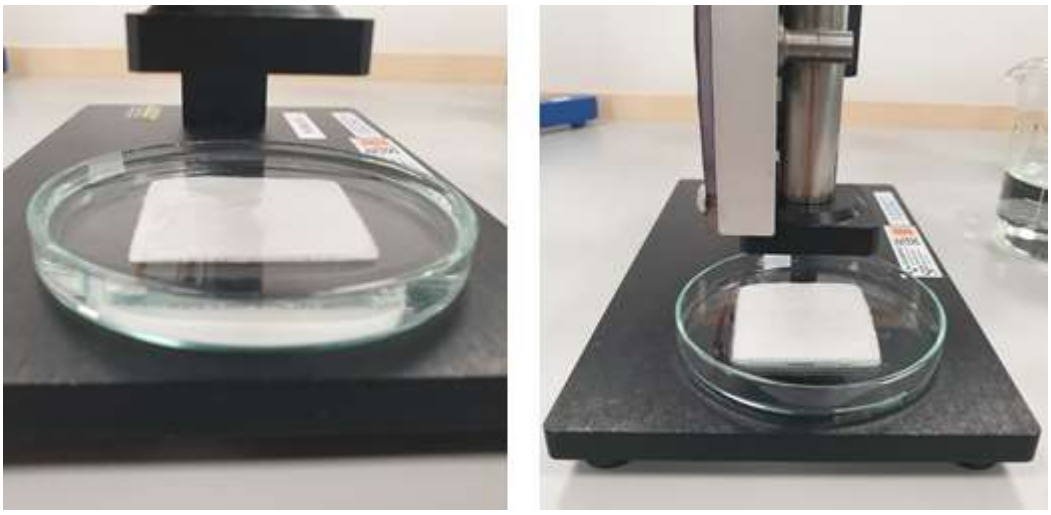

Fig 2: Example of thickness gauge equipment. Left) a submerged fibre network sample. Right) a saturated fibre network sample.

The extremely deformable nature of this type of material led to the need for extra considerations and care when handling or measuring samples, especially for very low solid volume fraction samples and for measurements of unloaded solid volume fraction. Measurements or testing under even the slightest load inevitably led to some degree of non-reversible deformation. Therefore, repeated measurements of the same sample were avoided as this will not lead to the same result due to deformation of the network. Extreme care had to be taken when handling, transporting, storing and placing the sample flat in the measuring equipment in order not to introduce unwanted deformation of samples. Due to the moisture sensitivity of contact mechanics of fibre-fibre contacts within the sample, all testing was performed in a controlled environment of 23℃ and RH 50%. Measurements intended to characterize the unloaded network solid volume fraction required extra considerations and meticulousness. Care had to be taken to ensure that the sample was perfectly flat on the underlying surface without flattening the sample in such a way as to introduce deformation of the network. Another implication in this type of solid volume fraction measurements is (unlike in the simulated results) that one cannot measure only in the bulk of the material in order to eliminate edge effects. Such effects include increasing or decreasing the solid volume fraction close to the top and bottom edges of the sample. In the measurements performed this was countered by using samples of high areal density to reduce the impact of such edge effects on the overall measured solid volume fraction. With these considerations taken into account, it was possible to achieve relevant and accurate results.

4.2 Formulation of the numerical framework

In modelling mechanics of non-bonded, semiflexible, anisotropic fibre networks on a fibre-level, there are several challenging requirements on the numerical framework in order to capture the dominating mechanical processes in a satisfactory manner. First, it is essential for the framework to represent the geometry and mechanical properties of fibres in a relevant way while accommodating a sufficient number of fibres to form a representative network. Second, the framework needs to properly represent the mechanics of fibre-fibre contacts, the relative translation and rotation of fibres as well as the emergence and breakage of fibre-fibre contacts. The latter phenomenon poses a critical computational challenge for any choice of numerical framework. Due to the nature of semi-

flexible non-bonded fibre networks, changes in fibre-fibre contacts are driving the mechanical response and deformation of networks under both tensile and compressive stresses. During compression of networks, the number of fibre-fibre contacts per fibre can often increase more than tenfold and result in fibres having the average distance between contacts with other fibres shrink as low as close to a single fibre diameter apart. This places great requirements on the model to accurately detecting the emergence and breakage of fibre-fibre contacts in a computationally efficient way. The efficiency of the contact search algorithm is therefore crucial to consider when choosing a numerical framework, as this step of the calculations is oftentimes the most computationally costly. The closely spaced contacts also lead to a need for finely resolved fibres to accurately describe fibre deformation. Aside from fibre properties, another area of importance is a generation of a realistic network and capturing the impact of network properties such as heterogeneity, fibre orientation, among others, on the mechanics of the network.

In this work we have used a numerical framework based on the Discrete Element Method (DEM) to model individual fibres. The fundamental element within DEM is an individual particle and the method goes into particle motion and particle-particle interactions. These interactions can take various forms, such as contact interactions in the normal direction (compressibility of particles) and tangential direction (friction between particles). Particles may also be bonded together to form structures, such as fibres, interacting with each other through linear or nonlinear forces or torques. The law governing this system of particles is the conservation of linear momentum and angular momentum:

$$m_i \ddot{\boldsymbol{r}}_i = \sum_j \boldsymbol{F}_{ij} + \boldsymbol{F}_i^B$$
$$\boldsymbol{I}_i \ddot{\boldsymbol{\theta}}_i = \sum_j \boldsymbol{T}_{ij}$$

where m_i is the mass and $\ddot{\boldsymbol{r}}_i$ is the acceleration of the i-th particle, $\boldsymbol{F}_{ij}$ is the interaction force between the i-th and j-th particle and $\boldsymbol{F}_i^B$ is the body force acting on the i-th particle. For the angular momentum, $\boldsymbol{I}_i$ is the moment of inertia tensor, $\ddot{\boldsymbol{\theta}}_i$ is the angular acceleration and $\boldsymbol{T}_{ij}$ is the interaction torque between the i-th and j-th particle. In this work fibres are modelled as a string of connected spherical particles. Particles constituting a fibre are spaced one diameter apart and linked by bonds with stiffnesses in the normal, shear, twist and bend modes. While non-bonded particles can interact by normal and tangential contact forces, for bonded particles the contact interaction is disabled and the interaction forces, $\boldsymbol{F}_{ij}$, and moments, $\boldsymbol{T}_{ij}$, come from the bonded interaction.

The equations for conservation of linear momentum and angular momentum are solved by time integration through the following process:

1. Apply initial conditions for positions and velocities of particles.
2. Run the contact search algorithm.
3. Calculate all forces and torques according to particle–particle interaction rules.
4. Calculate accelerations from the forces for each particle.
5. Calculate velocities and positions at the next time step for each particle.
6. Go back to step 2.

To generate realistic initial networks for use in the simulations, fibres are spawned randomly in a dilute suspension and deposited by gravity onto a wall element using the DEM framework to form a mechanically stable anisotropic fibre network of low solid volume fraction with similar characteristics to what is commonly seen in papers, hygiene products and nonwovens. An illustration of typical fibre and fibre network used in this work can be seen in Fig 3.

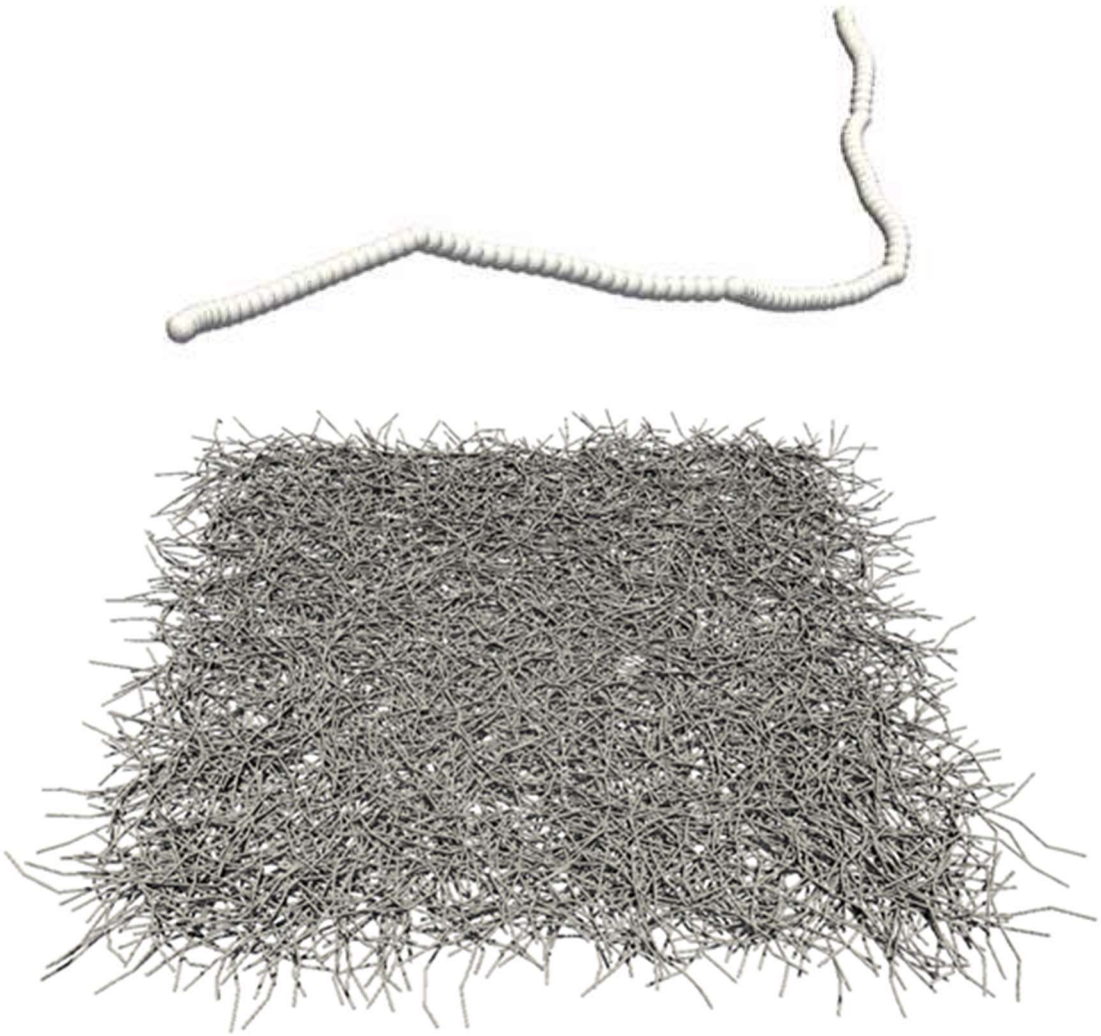

Fig 3: Illustration of a fibre modelled as a string of 110 connected particles (above) and a fibre network consisting of such fibres (below). The network is viewed at an angle from above and consists of 3000 fibres with a length of 2 mm deposited in a 1x1cm area.

Mechanical testing of the simulated networks under, for example, tensile or compressive deformation can then be performed using the generated network structure. In this work we have primarily focused on uniaxial compression and unloading of networks that is simulated by having an upper wall element compressing the network from above, while registering the pressure in the confining wall elements.

Some benefits of using this numerical framework include that fibre features and properties can be represented in a flexible way. Fibre geometry, such as its diameter and length, can be controlled by the diameter and number of particles used to form a fibre, while fibre curl, kink and twist can be controlled by the relative position between particles in equilibrium. The mechanics of fibre-fibre contacts is modelled by the contact force model for particle-particle contact and can represent various forms of contact interactions, such as elastic and elasto-plastic transverse compression, friction and adhesion between fibres. Mechanical properties of the fibres can be modelled by defining appropriate material-specific interactions of the particle–particle bonds within a fibre in order to represent different fibre deformation modes, such as fibre stiffness in normal, shear bend and twist modes. Being a particle-based approach, DEM inherently handles the relative translation and rotation of particles, as well as the emergence and breakage of particle-particle contacts. Using

the approach of fibres consisting of spherical particles spaced one diameter apart leads to fibres being relatively finely resolved with position nodes spaced one fibre diameter apart. Spherical particles are also the most computationally efficient particle shape for contact search algorithms.

However, some considerations related to the framework that required extra attention in the course of this work are worthy of notice. Due to the representation of fibres as a string of spherical particles some questions arise. The cross-sections of the fibres are inherently circular, not allowing for the modelling of alternative cross-sectional shape of fibres. This raises the question of how to choose a representative fibre diameter and how to calculate a representative volume when modelling fibres, like wood-based pulp fibres, that do not have a perfectly circular cross-section. For calculating the representative volume of a modelled fibre, it has in this work been seen as most fitting to assume a fibre volume equal to the cross-sectional area of the constituent particles times the fibre length, as opposed to the volume of the constituent particles. For choosing a representative fibre diameter it was deemed as most appropriate to represent fibres in such a way that the cross-sectional area of the fibre matches that of the physical fibre modelled. This approach allowed us to ensure that the volume occupied by the fibre in a simulated network matches that of the physical fibre and hence an accurate estimation of solid volume fraction of a modelled network. This is based on the long-known dependence of network mechanical response on the network solid volume fraction, such as the relationship between pressure and solid volume fraction shown in the work of van Wyk.[2] Another implication of the representation of fibres as a string of particles was that the approach inevitably introduces a slight effective surface roughness of the fibres which will have to be taken into consideration. Alternative approaches exist, such as the one that connects particles at less than one diameter apart in order to reduce the effective surface roughness of the modelled fibre. Such an approach, however, introduces additional complications in representing fibre contact mechanics due to overlapping particles. In this work we have chosen to model fibres using particles spaced one diameter apart while acknowledging the existence of a certain surface roughness. Motivation for this is twofold. The effect has been studied by Picu and Subramanian showing no impact of artificial friction for a similar system.[10,26] Additionally, the pulp fibres replicated in experiments are also not perfectly flat and inherently have a degree of surface roughness.

Another point that we had to consider when modelling fibre networks using the chosen modelling approach was balancing the kinetic energy and the damping in the system. The excess kinetic energy can lead to unphysical behaviour and oscillations in the network while excess damping in the system can lead to artificial forces in the network and excessive computational cost for allowing the system to settle to a near-static equilibrium (the state we are predominantly interested in in this work). Approaches used in this work for handling the identified problems included stepwise deformation (for example during simulated network compression), compressing walls are moved in sequences of slow compression followed by enough relaxation time to allow the network to dissipate kinetic energy and settle to a near-static equilibrium. During the simulations it was essential to monitor the kinetic energy and fibre deformation energy in the system to ensure that the network had reached this near-static state and was not expressing unphysical behaviour. Measurables monitored included the total kinetic energy, which should be allowed to reach a near-constant value, and the ratio between the total kinetic energy and fibre strain energy in the system, suggested by Abd El-Rahman and Tucker to be less than 0.1 for a quasi-static system.[27] Additional measures included monitoring the rate of change in individual fibres to ensure that all the fibres were stable or decreasing in kinetic energy. Another way of monitoring employed was looking at the average kinetic and fibre strain energies when sweeping over the network in the x, y or z-direction. In case of an external stress on the network, opposing stresses were monitored and should have settled at a near-constant value

and cancel each other, e.g., under uniaxial compression, the pressure on the top wall and bottom wall should have settled at near-constant values and cancel each other out.

The final requirement for successfully carrying out a project would prove to be patience. The countermeasures applied to unphysical behaviour of the system, i.e., reduced rate of deformation and increased relaxation times, while effective in reducing the artificial kinetic energy led to large computational cost with each simulation typically requiring significant computational time.

4.3 Theoretical considerations

Models developed from studies of statistical geometry of fibre networks are frequently used in research and industry alike. This type of models, while often subject to some limiting assumptions like a constant fibre length, fibres assumed rigid or no fibre rearrangement, has turned extremely useful for understanding fibre network behaviour. In this work we make use of some such models in order to support our experimental and numerical findings with theoretical explanations. This includes using the well-established relationship between pressure and solid volume fraction by van Wyk where the relationship is used to characterize network deformation and interpolate data between known datapoints.[2] Extrapolation of data based on the van Wyk expression can also be viable as long as the network is within the bending dominated regime. Another such model of great importance is the random contact equation to describe the relationship between the solid volume fraction and the number of fibre-fibre contacts.[3,5] This equation is useful in combination with experiments where the relationship can be used to estimate the number of fibre-fibre contacts in a network which is otherwise difficult to determine experimentally. Another application of the equation used in this work is the formulation of equations for estimation of the theoretical maximum unforced packing of networks.[5,20] This was done by combining the random contact equation with the theory related to the concept of caging number, the latter defined as the average minimum number of randomly placed fibre-fibre contacts on a single fibre that immobilize all its translations and rotations. The concept of maximum unforced packing was used in this work in relation to numerical results to further understand network structure in relation to this theoretical network configuration.

5. Selected results

The selected results mirror not only the achievements during the course of this work, but also the emergence of new research questions and the development of ideas on how to solve them. We were initially focused on obtaining important information in relation to network deformation and fibre deformation mechanisms of pulp fibre networks in tensile and uniaxial loading. The obtained results further highlighted the relevance of unloaded network solid volume fraction on network deformation and provided important indications related to the origin of changes of this parameter. It was then straightforward that the work advanced into explaining the mechanisms behind changes to the unloaded solid volume fraction in two of the most relevant cases of change, due to uniaxial compression and transitioning from a dry to wet state.

5.1 Paper I

In hygiene products such as diapers and tissue, mechanical responses under uniaxial compression are an integral part of both product properties and production, whether in the form of a baby sitting on a diaper or a compression unit in the production process. Understanding the deformation mechanism and the impact of fibre and network properties, therefore, has a direct impact on product and process development for this class of products. In Paper I, we investigated uniaxial compression of non-bonded anisotropic fibre networks with fibres oriented mainly in the in-plane direction, with a relatively soft transverse compressibility, based on measurements of pulp fibres. In this paper we used density to characterize the packing of the network instead of the closely related solid volume fraction, however, the results from both measurements on pulp fibre networks and the simulations using the numerical framework (Fig 4) followed the expected development of pressure in relation to the solid volume fraction from van Wyk, showing a power law type constitutive relation.[2]

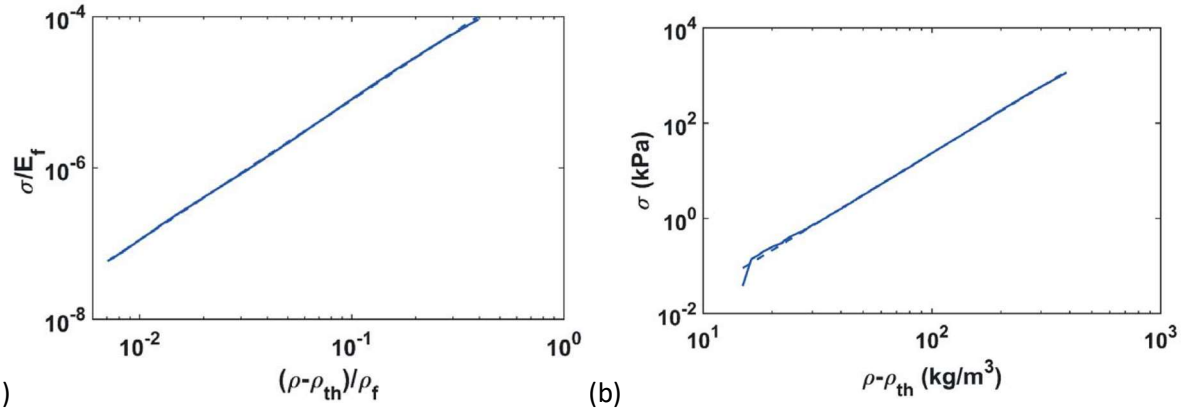

Fig 4: Stress-density relationship with power-law fitting (in log-log scale) (a) simulation results, (b) experimental results. Fitting is represented by the dashed line.

Next, we investigate the components of fibre strain energy stored in the normal, bending, shearing, twisting and fibre-fibre contact deformation modes during compression, shown in Fig 5.

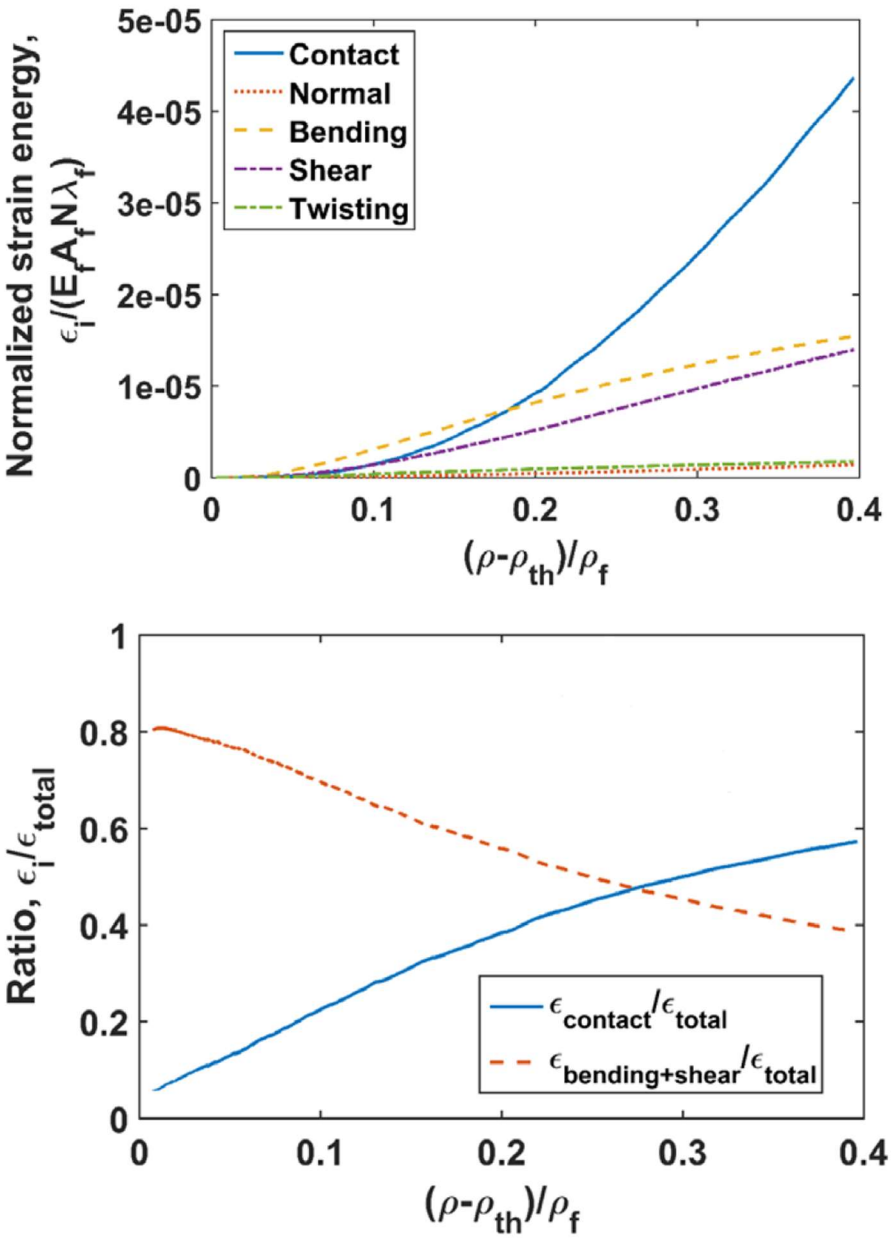

Fig 5: Partition of normalized strain energy, where ϵ_i represents the strain energy in each deformation mode. In these figures ρ is the network density and ρ_f is the fibre density, hence ρ/ρ_f is an alternative way of writing solid volume fraction. Here the x-axis is also compensated for the unloaded threshold density of the network ρ_f.

While the anisotropic fibre network still shows the general power-law-type constitutive relation in uniaxial compression, we note an interesting difference in the fibre deformation mechanism for this network. Fig 5 shows the different components of the fibre strain energy stored in the normal, bending, shearing, twisting, and fibre-fibre contact deformation modes. In the low compression range, bending and shear deformations make the major contribution similar to earlier studies on isotropic networks.[10] In the high compression range, however, the fibre-fibre contact energy makes the most significant contribution. This is in contrast to the literature results for the isostatic tri-axial compression of the initially isotropic fibre networks, where the contact energy is negligible as compared with bending and normal deformation modes.[10] The rationale for this, at least in the system studied here, is that the fibres are more oriented in the plane direction so that fibre-fibre contacts naturally take the uniaxial compression load, whereas fibre normal-directions are very much

oriented in the plane perpendicular to the compression. In addition, unlike previous studies, fibre-fibre contacts are much softer and can therefore compete with the bending deformation mode.

These findings brought new insights into the fibre deformation mechanisms dominating for uniaxial compression of this type of anisotropic networks at high degrees of compression, insights valuable for development of products consisting of such networks. Additionally, these findings would later provide valuable insights regarding the origin of permanent deformation due to uniaxial compression of this type of networks.

5.2 Paper II

Structural integrity of the network when subjected to tensile load is closely related to both product and production performance in the development of hygiene products such as diapers and tissue, and issues such as web breakage during production or core crumbling of diapers during use are serious concerns in product and process development. In Paper II, again using density to characterize packing of the material, we investigated network stiffness, strength and strain-to-failure of low-density networks under tensile stress. We used a deposited fibre network, compacted to a range of volume fractions relevant for the types of hygiene products studied in this work, in effect varying the number of fibre-fibre bonds holding the network together.

Studying results for network elastic modulus E, assuming $E \propto (\rho - \rho_{th})^n$, we find that the exponent n was not constant but changed slightly from 2.16 to 1.69 (Fig 6a).

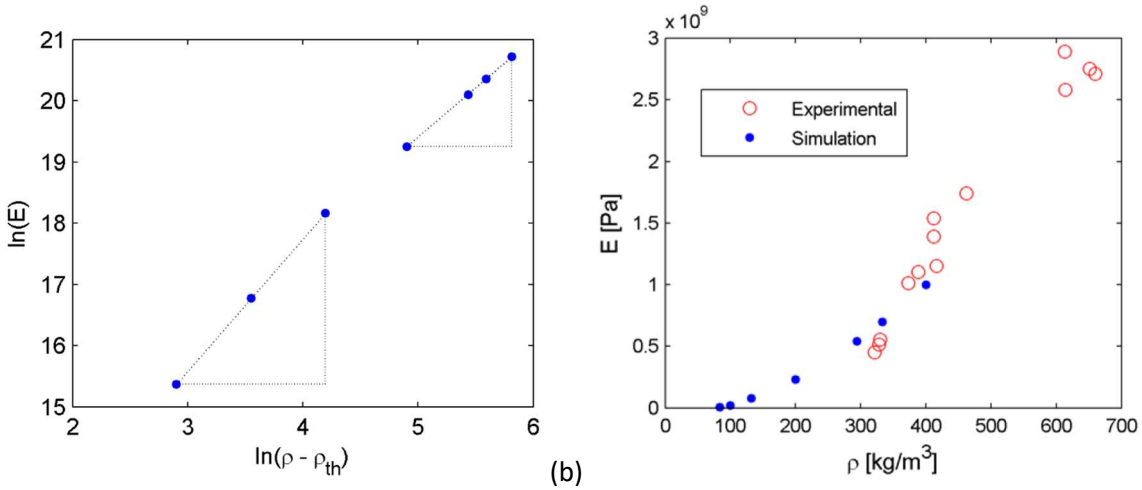

Fig 6: Elastic modulus of network as a function of network density. (a) Shown in ln-ln scale. (b) Comparison to experimental data.[28]

The results may correspond with the transition behaviour seen in the work by Licup with changing values of the exponent from 2 in the lowest density range to 1 in the highest density range.[29] A comparison to experimental data from Rigdahl and Hollmark (Fig 6b) shows that the simulated results cover a lower density range of the elastic modulus vs. density curve of typical paper sheets very well.[28]

The distribution of total fibre strain energy in the network as a function of density (Fig 7) also shows that in the lower density range, most of the strain energy is indeed stored in the fibre bending mode, whereas in the higher density range, it is in the fibre stretching mode.

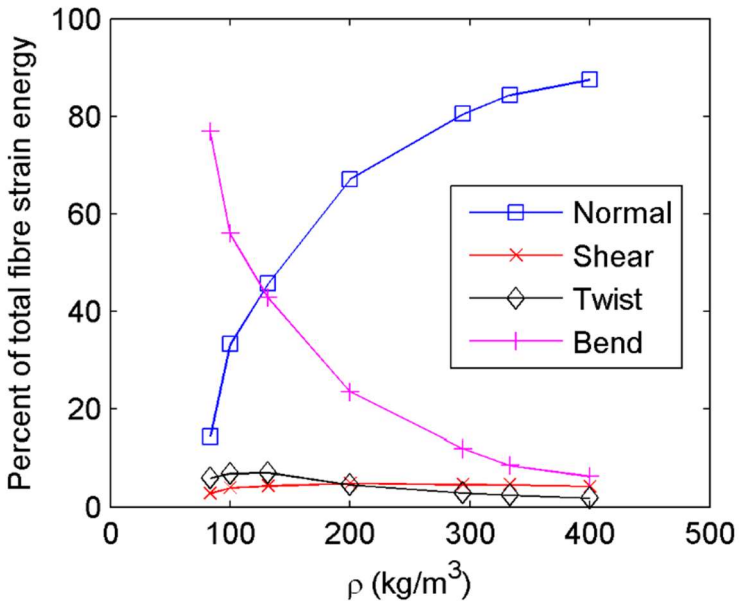

Fig 7: Distribution of total fibre strain energy during deformation for networks with varying density.

We proceeded to look at the results for network strength as a function of density and bond strength using the same seven virtual networks. In simulations we varied bond strength by multiplying the same factor to all four modes of the bond strength values. The results suggested that the density, $\rho - \rho_{th}$, and shear bond strength, τ_b, are separable as variables, and the dependence of network strength, σ_c, is generally expressed as:

$$\sigma_c \propto (\rho - \rho_{th})^m \cdot \tau_b^l$$

All data collapse very nicely as seen in Fig 8a, with the exponents m = 1.88 and l = 1.08.

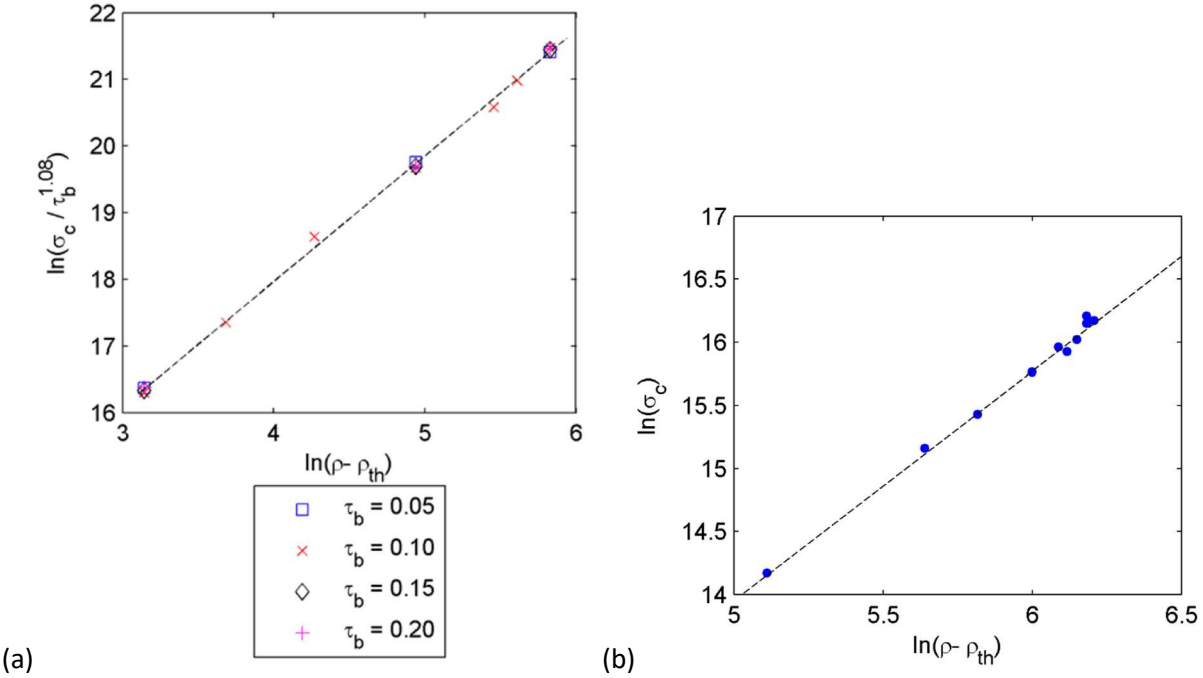

Fig 8: Network strength as a function of network density. (a) Simulated results normalized by bond strength. (b) Experimental data from Eriksson.[30]

To compare the simulated results to experimental data from literature we used data from Eriksson.[30] When we fitted the data with a power-law dependence $\sigma_c \propto (\rho - \rho_{th})^m$ with the same threshold density value as the simulation ($\rho_{th} = 63.3\ kg/m^3$), we found the exponent m = 1.82. The value showed an excellent agreement with the value of the exponent from the simulation m = 1.88.

Finally, we plotted strength vs. strain-to-failure, the so-called "failure envelope", in Fig 9.

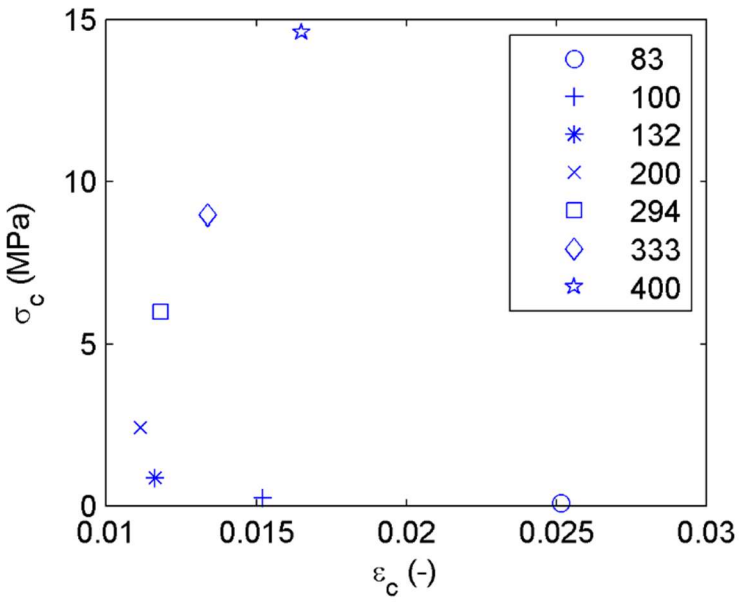

Fig 9: The failure envelope, network strength vs strain at failure, for simulated networks with varying density.

The results show a C-shaped relationship which corresponds with experimental results from the literature finding that the failure envelope of wet web strength of hardwood kraft pulps forms a "C-shape" for wet sheets with varying density.[31]

In conclusion, the simulation results for elastic modulus, strength and strain-to-failure showed excellent agreements with the respective experimental data in the literature. The scaling result of elastic modulus with density showed the typical transition from bending to stretching with changing values of the exponent previously shown in literature. Strength, however, showed scaling with density with a constant exponent within the density range investigated. The results (while expressed in terms of density above) imply the extreme importance of network solid volume fraction in the unloaded state (by directly affecting the number of fibre-fibre bonds holding the network together) and the strength of these bonds on network response to tensile deformation. This highlights the importance of accurately describing these two parameters when modelling these systems. However, given an accurate description of number of fibre-fibre bonds and bond strength it is noteworthy that the 3D-effects on mechanical properties (shearing, twisting of fibre and emergence of new fibre-fibre contacts) were found to be marginal in tensile deformation while in the case of uniaxial compression, the 3D effects were very significant, as discussed earlier. This highlights a difference in terms of modelling response to deformation for these networks and should be taken into consideration when choosing numerical framework.

5.3 Paper III

The importance of network solid volume fraction on network behaviour for both mechanical properties and fluid transport properties is well known from literature. This importance, especially in the unloaded state, is also highlighted in Paper I and II. For uniaxial compression the crucial impact of the unloaded solid volume fraction is seen by the dependence of pressure development on the

threshold density, ρ_{th}. In tensile deformation the importance is seen by the number of bonded fibre-fibre contacts, directly dependent on the solid volume fraction, being a prime source of network strength. In addition to this importance of accurately describing the unloaded solid volume fraction of networks in order to understand network behaviour, networks of this type are known to be extremely deformable and prone to non-reversible deformation. This leads to understanding of changes to the unloaded solid volume fraction of networks becoming paramount.

In this paper we studied numerically and experimentally non-reversible deformation of anisotropic, semi-flexible fibre networks due to uniaxial compression. The focus was to further the understanding of the physics behind permanent changes to the unloaded solid volume fraction by using the numerical framework to describe and quantify the effect of fibre rearrangement, elasto-plastic fibre contacts and fibre-fibre adhesion on non-reversible deformation.

Experimentally, measurements were performed to look at characteristic behaviour of fibre networks during uniaxial compression. The networks tested consisted of air laid Southern Pine pulp fibres, a type of fibre network often found in hygiene products such as diapers, incontinence pads and feminine pads. Two cases of measurements were performed where different samples were compressed up to 10kPa and 1000 kPa, respectively. Each test consisted of two sequences of compressive loading-unloading in the same spot to characterize the development of pressure vs. solid volume fraction for two repeated loadings. The difference in the (close to) unloaded solid volume fraction between the first and second compression is the measure we use to establish whether the non-reversible deformation i.e., change in the unloaded solid volume fraction of the network was obtained. Experimental results are shown in (Fig 10).

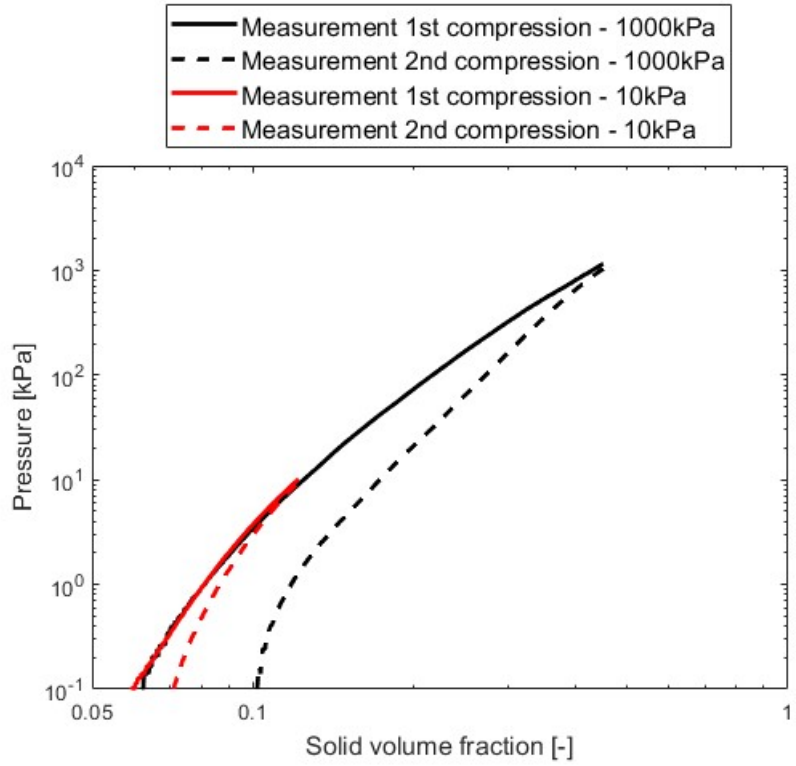

Fig 10: Pressure vs. solid volume fraction measured for two samples of pulp fibre networks. Each measurement consists of a sequence of two repeated compression–unloading cycles with the second compression intended to characterize the network deformation sustained from the first compression. The two different measurements are labelled 1000 kPa and 10 kPa based on the maximum pressure applied during compression.

In the investigated samples the initial solid volume fraction was 0.06 at the first compression. After compressing up to 10kPa, the initial solid volume fraction before the second compression had increased to 0.07, while compression up to 1000 kPa increased the initial solid volume fraction more, to 0.10.

In summary, the measurements show a significant impact on non-reversible deformation from the first compression through the entire pressure range tested, both for the tests with low and high maximum compressive forces.

In the next stage of this work the numerical framework was used to replicate the experimental procedure using a virtual network with fibre and network parameters based on the physical sample from the experimental testing. By repeating the experimental procedure using varying contact mechanics of the simulated fibres, the impact on non-reversible deformation from the different forms of fibre-fibre interaction can be characterized. Four different cases were simulated (with the findings outlined below) and with gradually introducing the complexity of the involved phenomena: i) networks with elastic contacts only, ii) networks with elastic contacts with adhesion, iii) networks with elasto-plastic contacts and, finally, iv) networks with elasto-plastic contacts and adhesion.

i) Network properties if only elastic contacts are assumed

We began by using an elastic contact model to study compression and non-reversible deformation in a fibre network. The use of fully elastic fibres leads to that the only source of non-reversible deformation is coming from fibre rearrangement, i.e., fibres sliding in relation to each other due to the deformation and finding a lower resting place after unloading leading to an increase in the solid volume fraction.

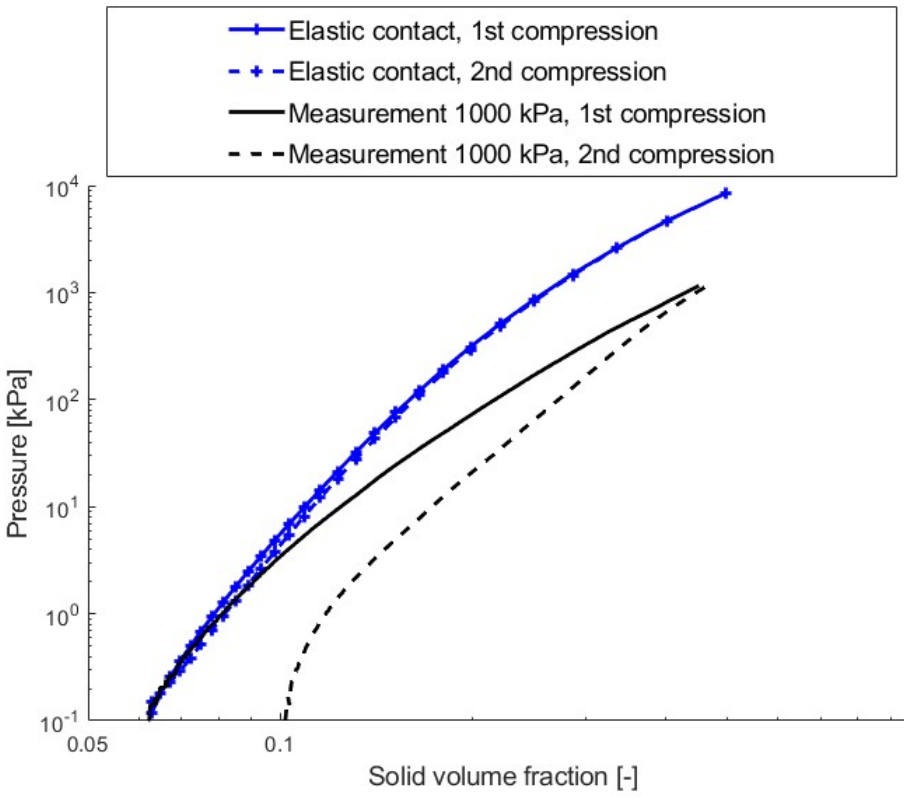

Fig 11: Simulation vs. measurements of the first and second compression. The simulated network involves only elastic contacts. The simulated results show that for the chosen network the pressure development for the second loading overlaps with that of the first loading. This indicates that there has been no non-reversible deformation caused by the first loading in the simulated results.

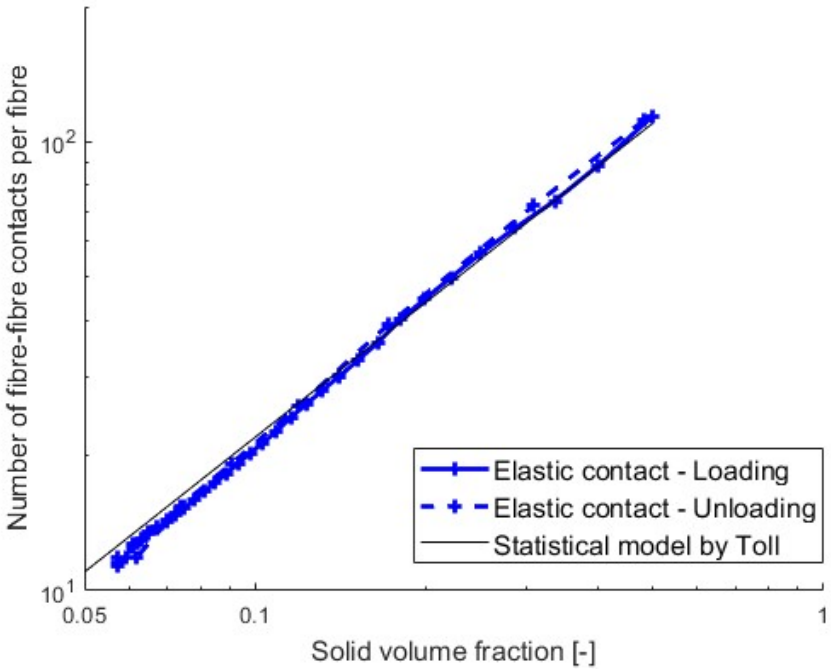

Fig 12: Number of fibre-fibre contacts per fibre for the simulated network with elastic contacts during loading (solid blue) and unloading (dashed blue). A statistical model by Toll (black) is presented as a reference. The results show the number of fibre-fibre contacts during unloading overlapping with the loading curve and returning to the original number of fibre-fibre contacts after unloading.

The results of pressure vs density (Fig 11) show that for the second loading of the simulated network the pressure starts at the same SVF as for the first loading and that the pressure curves for the two loadings follow each other very closely. This behaviour differs from the measured characteristics, where the second loading starts having pressure at a significantly higher SVF than for the first loading (Fig 12). Also, the pressure for the second compression is reduced compared to the first loading for the entire range of solid volume fraction up to the point of maximum compression. Also looking at fibre-fibre contacts of the simulated network, (Fig 12), we see an extremely close correlation to the predicted values from the statistical model by Toll.[5] Comparing the simulated curves for loading and unloading, we see that the number of contacts during unloading retraces the path from the loading curve very closely, returning to the same number of fibre-fibre contacts after unloading as before compression.

These findings clearly indicate that in the simulated results there has been no non-reversible deformation due to fibre rearrangement caused by the first loading.

ii) Network properties for networks affected by elastic contacts with adhesion

The second step consisted of looking at compression of the same fibre network as in the previous section, but we now add inter-fibre adhesion to characterize the role that adhesion plays in non-reversible deformation of a network from a first compression. For the simulations we choose the maximum adhesive force between fibres to be 25µN based on the measurements by Andersson.[32] We compare the obtained results to the case where no adhesive forces are present. In addition, we will look at the effect of using an exaggerated effect of adhesion by a factor of ten, using the maximum fibre adhesive force of 250µN.

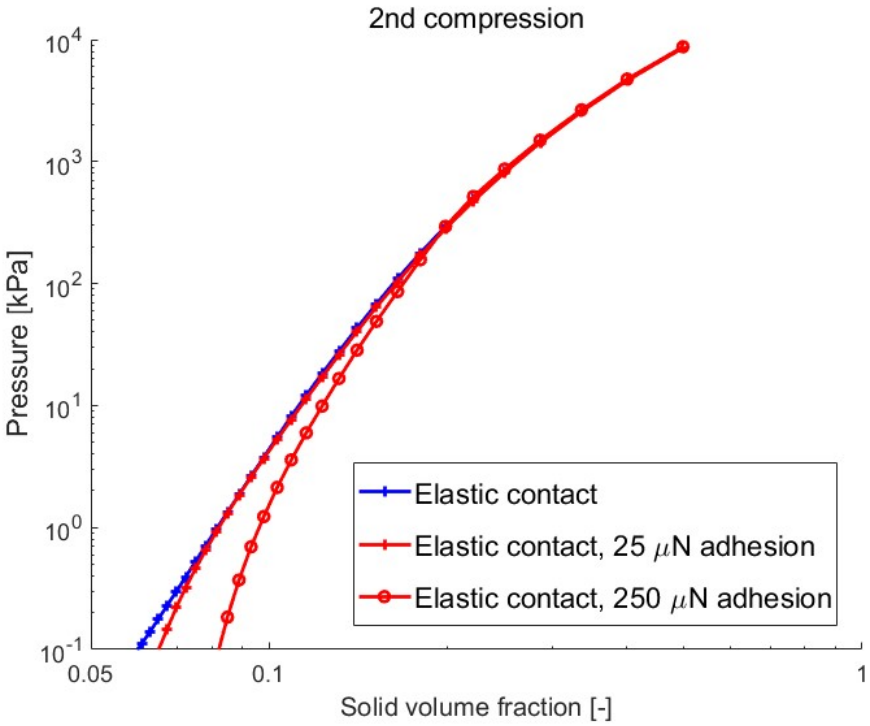

Fig 13: The simulated second compression of networks with varying inter-fibre adhesion. In all the cases the fibres have elastic contacts. The increased magnitude of the adhesive force is seen to increase the degree of non-reversible deformation from the first compression in terms of initial solid volume fraction and decrease the pressures at low solid volume fractions.

Looking at the second compression of the network (Fig 13), we see some effect of the inter-fibre adhesion on non-reversible deformation of the network from the first compression. The initial solid volume fraction, measured at 0.1 kPa, for the second compression has increased from 0.06 to 0.065 and 0.08 for inter-fibre adhesion forces of 25μN and 250μN, respectively, compared to no increase in the network without fibre-fibre adhesion. The source of the non-reversible deformation is further clarified when looking at a number of fibre-fibre contacts per fibre during unloading of the network (Fig 14).

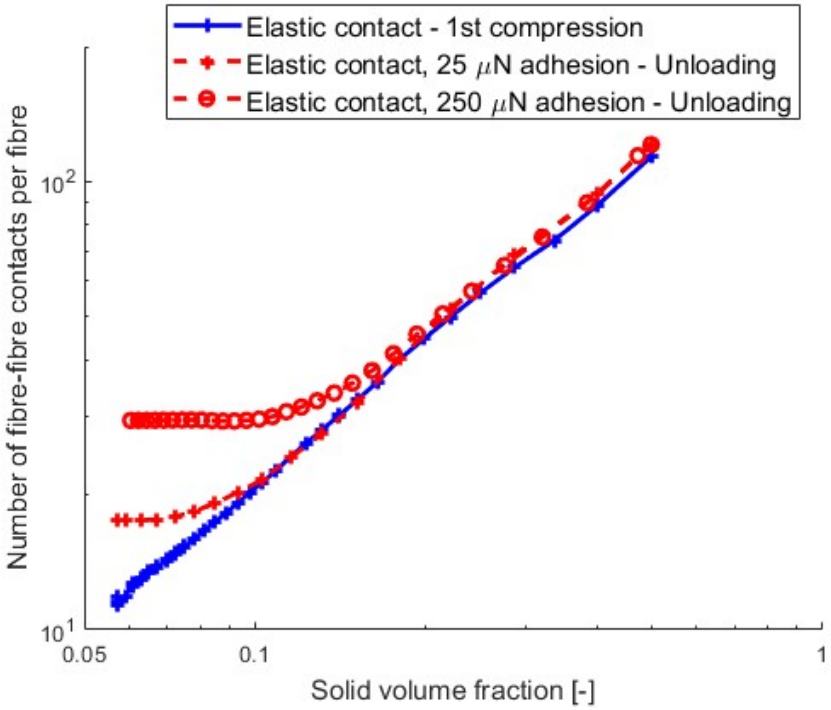

Fig 14: Number of fibre-fibre contacts per fibre vs. solid volume fraction during unloading for two networks with inter-fibre adhesion compared to the case with elastic contacts. The number of contacts closely follows the elastic case during unloading before settling at a plateau at a level dependent on the magnitude of the adhesive force.

If we follow the development of the number of fibre-fibre contacts during unloading (curves starting in the top right of Fig 14 going left) we see that, for the simulations with inter-fibre adhesion, that number initially decreases and closely follows the curve of the simulated case without adhesion. As the compressing wall is moved further, the solid volume fraction decreases and the curves for the cases with adhesion start to deviate from the case without adhesion leaving an increased number of fibre-fibre contacts remaining during unloading compared to the case without adhesion. As the compressing wall is moved even further away, the number of fibre-fibre contacts for the cases with adhesion settles at a plateau and the network loses contact with the compressing wall. The results are a clear indication of non-reversible deformation of the network and that the degree of non-reversible deformation is dependent on the magnitude of the inter-fibre adhesive force.

However, results for the simulation using 25μN adhesive force (literature value) show that the degree of non-reversible deformation of the simulated network is on a different level than what is seen in the comparable measurements (*1000 kPa* in Fig 10). Additional simulations also show that after compression-unloading to a maximum solid volume fraction of 0.12 (comparable to the *10 kPa* measurements in Fig 10) the number of remaining fibre-fibre contacts is on the same level as for the simulated case replicating the *1000 kPa* measurement, indicating that after a certain degree of compression no further non-reversible deformation is produced in the simulated network.

Based on these results, in combination with additional simulations with varying fibre stiffness, it is concluded that for the simulated networks with elastic fibres, inter-fibre adhesion has a certain impact on non-reversible deformation. The degree of non-reversible deformation is dependent on the relationship between the adhesive force and fibre stiffness, with the higher magnitude of the former and lower fibre stiffness leading to an increase in non-reversible deformation after compression. The impact of adhesion is, however, limited to a low solid volume fraction range where the adhesive force can overcome the fibre deformation forces and moments. For compression beyond this point, no further non-reversible deformation is sustained. This indicates that inter-fibre

adhesive forces help explain non-reversible deformation for compression in the low SVF range, such as seen in the measurements labelled “10 kPa” in Fig 10. The results also show that when using the adhesive force of $25\mu N$, no further non-reversible deformation is achieved for compression beyond solid volume fraction of around 0.1. Such a finding is not corresponding well with the measurements (see measurement labelled *1000kPa* in Fig 10), as it does not capture the deformation of the network due to compression to high solid volume fraction, suggesting the impact of physics not accounted for in the simulations happening at high solid volume fractions.

iii) Network properties for networks affected by elasto-plastic contacts

At this point it is concluded that the large non-reversible deformation seen in the measurements is not described well by the above modelling assumption for high degrees of compression. Based on the results from Paper I showing that fibre-fibre contact energy is the dominating fibre deformation energy for networks in this range we proceed to investigate the effect of plastic contact deformation on non-reversible deformation.

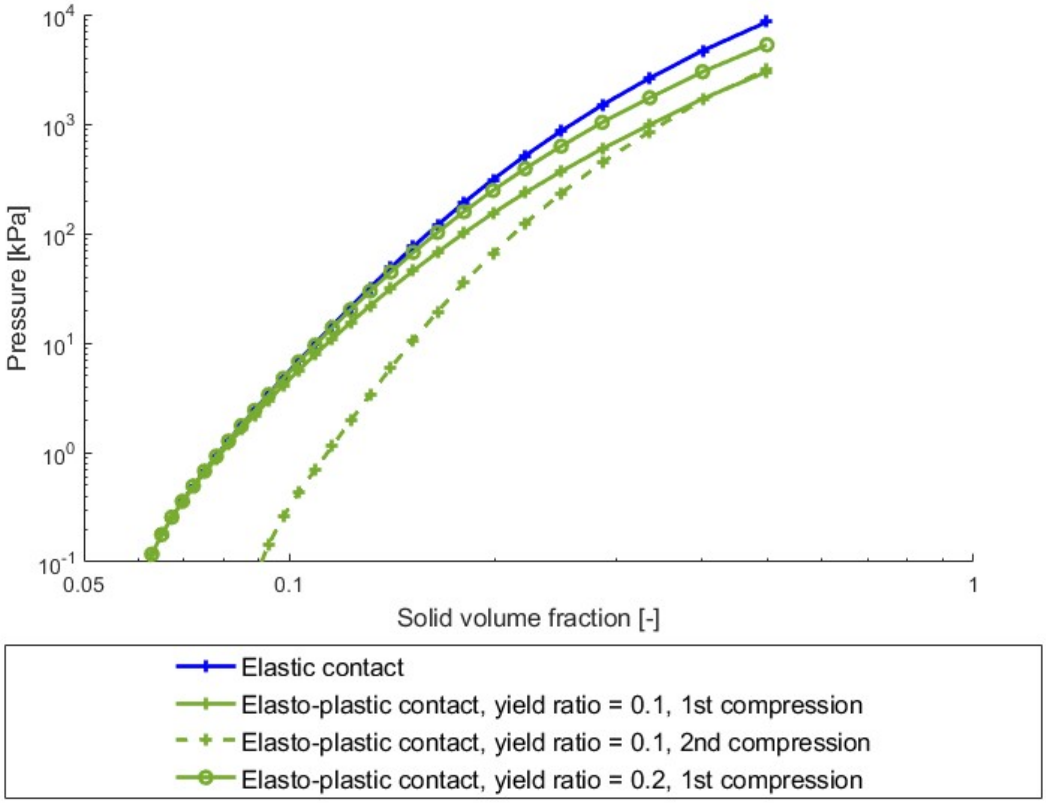

Fig 15: Simulated compressions of networks with elasto-plastic contacts compared to a network with elastic contacts. The results for the first compression show that the pressure is unaffected in the low SVF-range. At higher compression, the pressure is reduced compared to the simulated network with elastic contacts. For the second compression, the pressure vs SVF curve is shown for a yield ratio of 0.1. The results show reduced pressure compared to the first compression in the entire SVF-range up to the point of the maximum pressure, where the curves for the first and second compression coincide.

Results show that elasto-plastic contacts between fibres affect non-reversible deformation both in terms of pressure development and the initial solid volume fraction after compression of the network in the cases where the yield criterion in the contact points has been exceeded (Fig 15). The network pressure at high solid volume fraction is reduced compared to that in networks with elastic contacts. Also, for the second compression, the initial solid volume fraction is increased, and the network pressure is reduced compared to the first compression through the entire solid volume

fraction range up to the maximum pressure. All these findings are in good agreement with the characteristics of measurements of compression up to high solid volume fraction (see measurements labelled *1000 kPa* in Fig 10). However, as fibre networks with elasto-plastic contacts do not generate non-reversible deformation of the network for the cases where the yield criterion in the contact points is not exceeded, the elasto-plastic effect itself cannot replicate non-reversible deformation in the low solid volume fraction range such as the one seen in, for example, measurements labelled *10 kPa* in Fig 10.

iv) Network properties for networks affected by elasto-plastic contacts with adhesion

After concluding that the impact of adhesion could explain non-reversible deformation for compression in the low solid volume fraction range and that the impact of elasto-plastic contacts could be behind non-reversible deformation for compression in the high solid volume fraction range the next step is to look at the impact of networks with fibres having a combined effect of elasto-plastic contacts and inter-fibre adhesion.

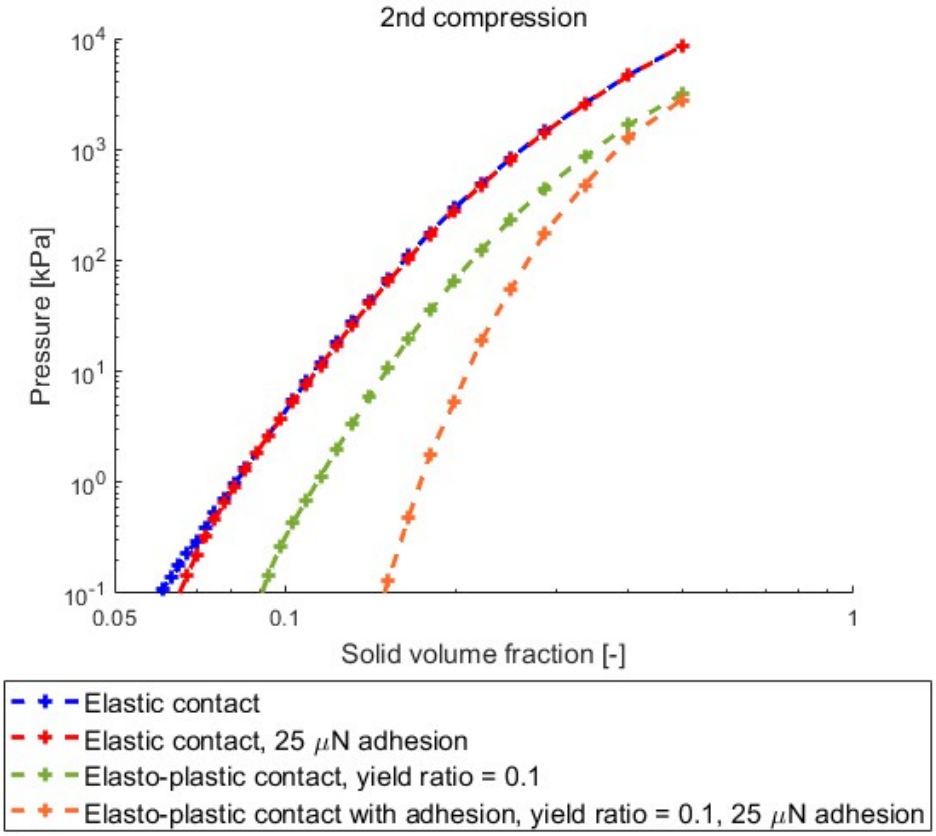

Fig 16: Pressure development vs. solid volume fraction for the second compression of a network with elasto-plastic contacts with adhesion, compared to the three networks from previous results: Elastic contacts, elastic contacts with adhesion and elasto-plastic contacts. The results show a significant impact on non-reversible deformation in the network with elasto-plastic contacts with adhesion, both in terms of reduction in pressure and increase in the initial solid volume fraction.

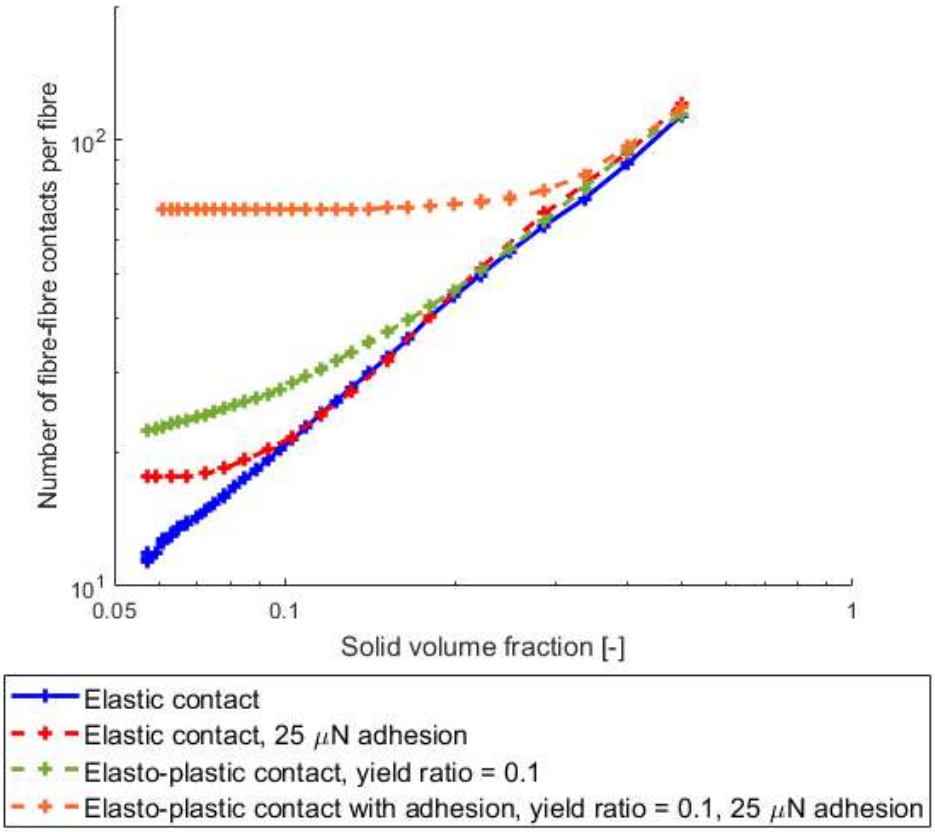

Fig 17: Number of fibre-fibre contacts remaining during unloading of a network with elasto-plastic contacts with adhesion compared to the three networks from previous results: Elastic contacts, elastic contacts with adhesion and elasto-plastic contacts without adhesion. The contacts for the network having elasto-plastic contacts with adhesion settle at a plateau of 70 contacts per fibre indicating a significant impact on non-reversible deformation of the network.

The results for the second compression of a network with elasto-plastic contacts with adhesion shows a notable impact on the pressure vs solid volume fraction curve compared to the first compression (Fig 16). The initial solid volume fraction, measured at 0.1 kPa, is increased from the original value of 0.06 to 0.15 showing significant non-reversible deformation and in essence reducing the network thickness to less than half the original thickness. For the simulated cases we note that, while adding inter-fibre adhesion to a network with elastic contacts gives only a marginal contribution to non-reversible deformation, adding the same effect to a network with elasto-plastic contacts results in a significant increase in non-reversible deformation sustained by the network and reduction in the development of the pressure for the second compression. This is further corroborated when studying the development of fibre-fibre contacts during unloading. Results show a very significant difference in fibre-fibre contacts retained after unloading for the case having the combined effects of elasto-plastic contacts with adhesion compared to the cases with only adhesive contacts or only elasto-plastic contacts (Fig 17).

Combining the effects of adhesion and elasto-plastic deformation of fibres clearly has an unambiguous synergetic effect. Plastic deformation of contact points during loading of the network reduces the fibre-fibre contact pressure and the effective fibre diameter in these points permanently in the simulation. The reduction in contact forces and the effective fibre radius leads to an increase in the retained adhesive contacts after unloading. In this way, the effect of inter-fibre adhesion is amplified by the plastic deformation in contact points. At the same time, adhesive contacts remaining intact lead to less rearrangement of fibres and contact points during unloading and during

a second loading of the network. This effect ensures that the fibre-fibre contacts during a second loading happen in the exact same spot where plastic deformation of fibres has occurred during the first loading. This works to transfer the full effect of plastic deformation from a first loading to the pressure development of the second loading.

Comparing network deformation behaviour to what was seen experimentally, the simulations with the combined effect of inter-fibre adhesion and elasto-plastic contacts show the ability to replicate characteristics of measurements. This is seen for compression to high solid volume fractions, as well as lower degree of compression both in terms of pressure development vs solid volume fraction and non-reversible deformation for first and second compressions of the network.

To conclude, the results and findings in Paper III highlight the everchanging nature of this type of material. Not only are the networks extremely deformable, but deformation also results in persistent change of the solid volume fraction even for the slightest of deformations leading to changes in macroscopic behaviour in terms of fluid transport properties and mechanical response. For networks with low solid volume fraction, non-reversible deformation is primarily sustained due to fibre-fibre adhesion. The effect of fibre-fibre adhesion, however, is limited to a solid fraction range where the adhesive forces can overcome the fibre deformation forces and moments. In a higher solid volume fraction range, plastic contact deformation can play a significant role. When plastic deformation of contact points occur, the plastic deformation reduces fibre deformation forces in contact points, acting to magnify the effect of fibre-fibre adhesion.

5.4 Paper IV

This paper concerns the spontaneous deformation of networks due to transitioning from a dry to a wet state. Given that the main functionality of many common products consisting of fluff pulp fibre networks require the absorption of liquids, network solid volume fraction in a wet state becomes a crucial component for controlling properties like permeability and capillary pressure, on which product function eventually depends. Therefore, in this fourth paper we focus on understanding the change in network solid volume fraction due to transitioning from a dry to a wet state.

In this work we will in the first stage use experiments to characterize and quantify the change in the network solid volume fraction for networks of varying solid volume fractions in the dry state when transitioning to a wet state. In the second stage we will compare experimental results with those obtained by our DEM simulations and identify the main physics behind the observed changes to the network solid volume fraction due to the transition. Finally, in the third stage, we will utilize results from the simulations in combination with theoretical considerations by other research groups to provide a comprehensive theoretical explanation regarding the network state to which the wet network transitions.

Experimental stage

Experimentally we performed measurements to look at the behaviour of the solid volume fraction of fibre networks when going from a dry to a completely wet state. The networks tested consisted of air-laid Southern Pine pulp fibres compressed to a varying degree by dry uniaxial compression in order to create networks with a varying dry solid volume fraction. In this study we chose to primarily focus on characterizing the change in the solid volume fraction of a network in the unloaded state (Base Case). To complement the measurement procedure, we have decided to use two additional approaches (termed Case II and Case III). For Case II we use the more commonly used approach of measuring thickness of this type of materials, which is under a slight pressure. For Case III we measure the solid volume fraction in a fully saturated state but not submerged in water, which will lead to the network being subjected to a slight deformation stemming from the capillary forces.

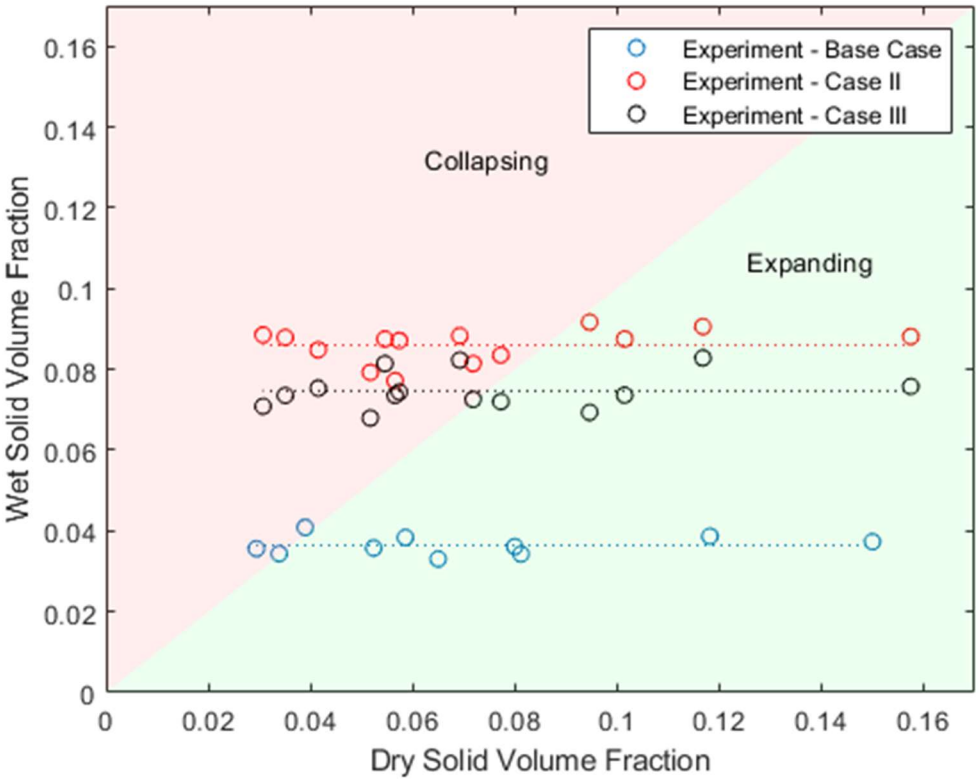

Fig 18: Experimental results and mean values of the networks in our work transitioning from dry to wet state, measured with Base Case (Blue), Case II (Red) and Case III (Black). The top left region (light red) signifies an increase of the solid volume fraction (collapse of the network on a micro-level) when going from a dry to a wet state. The bottom right region (light green) indicates a decrease of the solid volume fraction (expansion of the network on a micro-level) when going from a dry to a wet state. A consistent trend of the resulting wet solid volume fraction being independent of the dry solid volume fraction is observed in all three cases. The resulting level of the wet solid volume fraction, however, is proven very sensitive to the different loading cases in the wet state.

The experimental results (Fig 18) show the resulting wet solid volume fraction being independent of the initial dry solid volume fraction. The tending of the wet solid volume fraction to a close to the same value is seen in all three measurement procedures, Base Case (submerged and unloaded), Case II (submerged under 0.45 kPa load) and Case III (fully saturated and unloaded). The average values of the wet solid volume fraction, however, are shown to be very sensitive to the different loading cases in the wet state. Base Case exhibits an average wet solid volume fraction of 0.036, Case II yields an average of 0.086 and Case III has an average of 0.075.

The experimental results allow us to draw three important conclusions:

1. The state to which the network transitions when going from a dry to a wet state is independent of a prior dry solid volume fraction.
2. The level of solid volume fraction of networks in the wet state is extremely sensitive to the degree of loading of the network.
3. No fibre or network parameter that affects final packing of the wet sample has been affected by the compression of the network or the effect is annulled by the presence of water.

The shown reversion of networks with widely varying dry solid volume fractions to a single one and with the same network configuration when transitioned to the wet state brings important information regarding the source of non-reversible deformation sustained from the compression used to create networks of a varying dry solid volume fraction. The fact that for all three cases, both networks that have been compressed to a high degree and the uncompressed networks end up at

the same wet solid volume fraction, either by expanding or collapsing, allows us to conclude that no fibre or network parameter that affects final packing of the wet samples has been affected by the compression of the network or the effect is annulled by the presence of water. These result and conclusions are important in relation to our previous work in Paper III where we suggested the source of non-reversible deformation from dry compression to be a synergetic effect of inter-fibre adhesion and plastic deformation in fibre-fibre contact points. The results from the measurements in Fig 18 seem to further corroborate this assumption, indicating that the fibre-fibre adhesion in the dry state is annulled in the wet state supporting the suggested source of the inter-fibre adhesion to be due to moisture. Further, if plastic deformation of fibres plays a role, the effect must be either very local, acting only to amplify the effect of adhesion, or small enough not to affect the final packing of the wet sample.

Numerical stage

In this section we explain by our simulations the changes in the network solid volume fraction seen in the measurements when changing from a dry to a wet state (Fig 18). The goal is to identify phenomena and material parameters that play a role in the change of the solid volume fraction. Based on the findings in Paper III we hypothesize that in the dry state the fibre-fibre adhesion prevents low solid volume fraction networks from compacting due to gravity to a higher solid volume fraction packing. For high solid volume fraction networks, the same adhesion in combination with local contact deformation of fibres is what prevents fibres from reverting back to a relaxed state and the network to expand to a lower solid volume fraction packing. In the wet state adhesion disappears and both high- and low- solid volume fraction networks are tending to the same value of the solid volume fraction.

To investigate this, we model networks with fibre properties and a distribution of fibre lengths based on measurements from the same material as the measured sample but with varying degree of simulated compression, resulting in varying dry solid volume fraction.

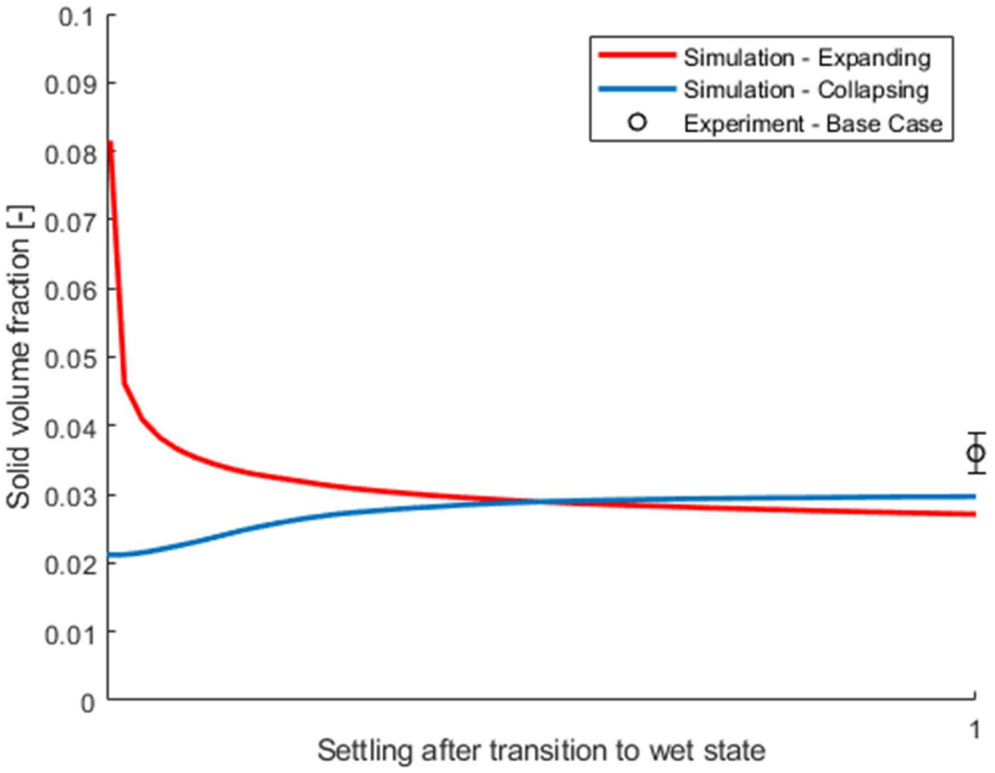

Fig 19: Simulation and experimental results of the solid volume fraction of networks settling after transitioning from a dry to a wet state. The red curve shows a compressed network with a high solid volume fraction in the dry state reducing in the solid volume fraction as it settles (the expanding network). The blue curve shows an uncompressed network with a low solid volume fraction in the dry state increasing in the solid volume fraction as it settles (the collapsing network). The results show the solid volume fraction after settling in the wet state tending to the same value. The horizontal axis is the simulation timestep normalized by the number of timesteps to reach the designated stop criterion, based on first and second derivatives being below a selected threshold value.

The simulation results in Fig 19, formulated to explain the findings from the experimental Base Case (submerged and unloaded network) show two simulations of the networks with the same composition but with different dry solid volume fractions (0.021 and 0.081, respectively). The results clearly show the solid volume fraction tending to the same value for the two networks in the wet state, showing a good agreement with the experimentally observed behaviour of the same wet-state solid volume fraction being independent of a dry-state one (Fig 18). The terminal (or the equilibrium) solid volume fraction for the simulated networks reaches the values of 0.030 and 0.027, respectively, which is within 30% of the corresponding measured wet solid volume fraction from Base Case with an average value of 0.036.

To further find out how the numerical simulations can explain the underlying physics, we proceed by replicating the Case II measurements in simulations by compressing the simulated network to a pressure equal to that of Case II measurements of 0.45kPa.

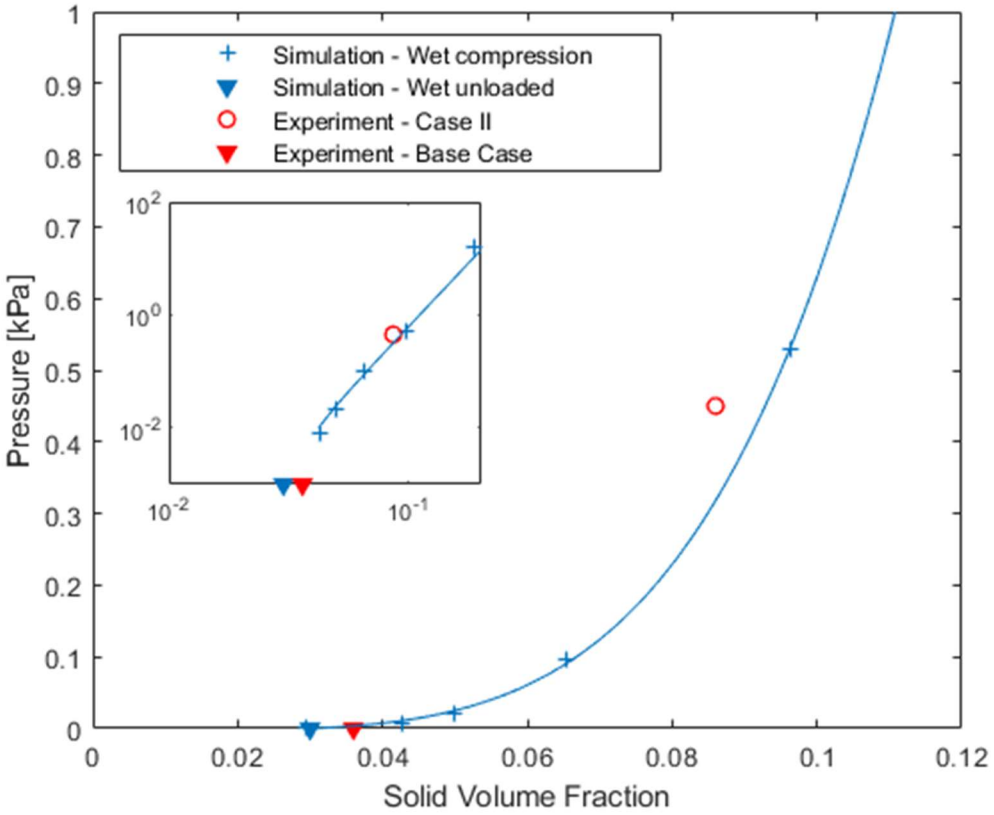

Fig 20: Measured solid volume fraction under 0.45 kPa (red circle) load compared to the simulated pressure vs. solid volume fraction (blue markers). The resulting solid volume fraction at 0.45 kPa shows a good agreement between the measured (0.086) and simulated values (0.092). Inset: Pressure vs. solid volume fraction for the same results in a log-log scale. The fitted line based on the van Wyk equation is added to guide the eye.[2]

The simulated results, (Fig 20), gives a solid volume fraction of 0.092 at 0.45kPa, agreeing well with the measured average solid volume fraction of 0.086 at 0.45kPa.

The shown agreement between the simulations and measurements, both in terms of the networks with varying dry solid volume fractions transitioning to close to the same wet solid volume fraction (Fig 19), and in terms of a value of the solid volume fraction to which the wet solid volume fraction transitions (Fig 20), allows us to conclude:

- The change in the network solid volume fraction from dry to wet state can be explained as driven mainly by the disappearance of fibre-fibre adhesion in combination with changes in fibre mechanical properties when wet.
- A non-reversible deformation in the dry state, creating high solid volume fraction networks, is for the range of compressions tested in this work mainly caused by the synergetic effect of adhesion and plastic deformation at contact points, corroborating the findings from Paper III.
- Low-solid volume fraction-networks in a dry state are prevented mainly by adhesion from compacting to a higher solid volume fraction packing.

Theoretical stage

The next step is to complement our experimental and numerical work with a theoretical explanation of the underlying phenomena when fibre networks transition from a dry to a wet state. Based on the conclusions above, we hypothesised that uncompressed networks with a low solid volume fraction in the dry state should in the wet state, due to disappearance of adhesion, collapse to the state of maximum unforced packing, defined as the limiting solid volume fraction above which application of

pressure resulting in deformation of fibres is required for random fibre networks in the absence of adhesion. Networks with prior compression, having a high solid volume fraction in the dry state, should on the other hand, upon disappearance of adhesion, have their constituent fibres revert to an unstrained state, while expanding the network up to the same state of maximum unforced packing.

To prove this hypothesis, we continue the analysis by looking at numerically obtained information on fibre contacts. The goal is to determine whether the state to which wet networks settle following our simulated dry-to-wet transition is in fact in agreement with the theoretical results for maximum unforced packing and stability onset for random packing of thin rods. We note, however, that the results from literature showing that the range of stability onset and maximum unforced packing is characterized by the average number of fibre-fibre contacts for fibres being close to the caging number were obtained for networks consisting of fibres with a constant fibre length.[5,20] When considering that the fibre aspect ratio impacts the average number of fibre-fibre contacts at a given solid volume fraction, (Eq. 1), we argue that we cannot automatically assume that the same results hold for networks consisting of fibres with varying aspect ratios. We have therefore chosen to carry out simulated dry-to-wet transitions similar to those outlined above, but this time with a constant fibre length. Our objective here is to be able to make a more direct comparison with theoretical findings obtained by other research groups and find out whether our numerical framework produces networks that indeed transition to the state of maximum unforced packing. To do so, we deposit two new networks with a constant fibre length of 0.8 mm (aspect ratio 37) and 2.0 mm (aspect ratio 93) based on the arithmetic average and length-weighted average fibre length from the measured sample in our experiments. We then repeat simulating the transition from a dry to a wet state in the same procedure as for the network with a varying fibre length and using the same fibre properties. For each fibre length we performed one simulation with an uncompressed network having a dry solid volume fraction lower than the maximum unforced packing and one simulation with a compressed network having a dry solid volume fraction higher than the maximum unforced packing (*Eq. 4*), in total four simulations (Fig 21).

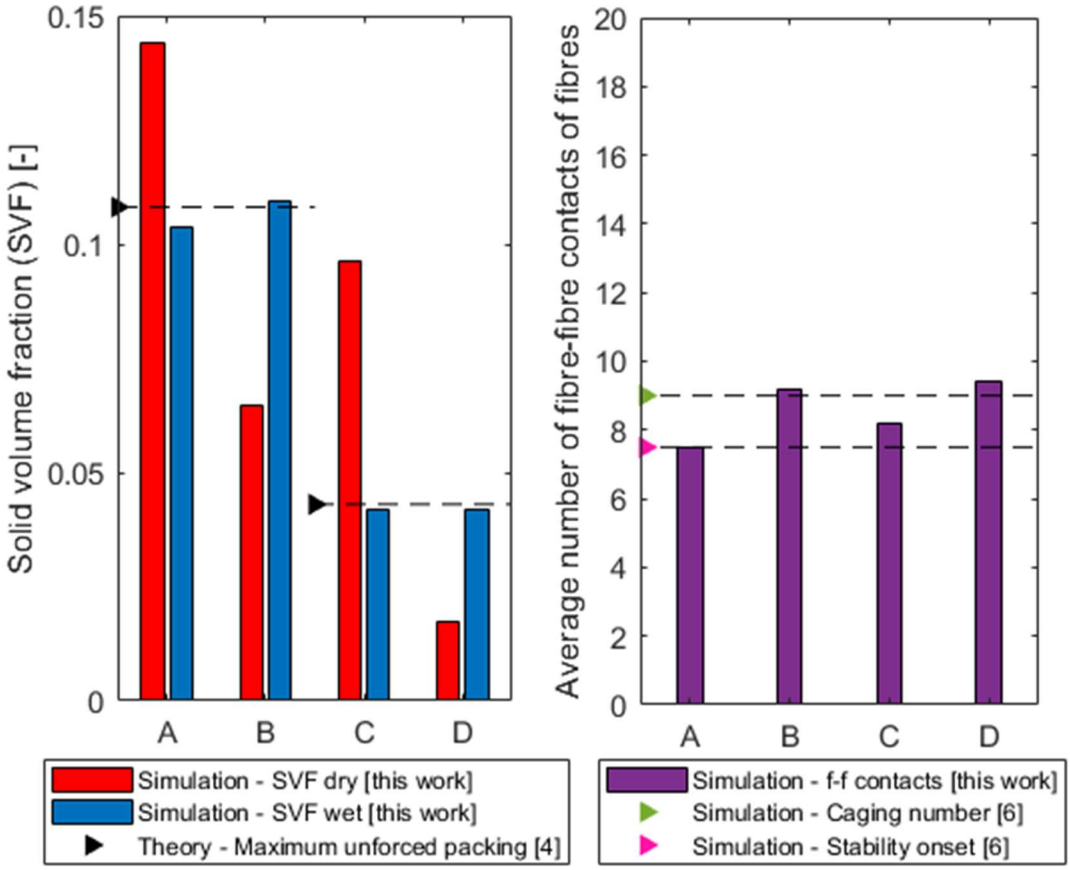

	L_f	Aspect ratio	Compression	Dry solid volume fraction
A	0.8 mm	37	Compressed	High
B	0.8 mm	37	Uncompressed	Low
C	2.0 mm	93	Compressed	High
D	2.0 mm	93	Uncompressed	Low

Fig 21: Results for four networks, A, B, C and D, transitioning from a dry to a wet state. The left-hand graph shows the results of the solid volume fraction of an initially dry network and of the solid volume fraction of the networks after transitioning to the wet state. The results show how the wet solid volume fraction is tending to the same wet solid volume fraction for the networks consisting of fibres with the same aspect ratio, A-B and C-D. The value of the solid volume fraction to which the network is tending is dependent on the aspect ratio and agrees well with the theory for maximum unforced packing from Toll.[5]
The right-hand graph shows the average number of fibre-fibre (f-f) contacts after transitioning to the wet state for the same four networks. The average number of contacts is in the range of 7.5 – 9.5, corresponding to what is given in the simulations of caging number and stability onset by Wouterse et al.[20]

The obtained solid volume fraction of the initially dry networks and the ones after transitioning to the wet state for the four networks show how the wet-state solid volume fraction is tending to the same level for the networks consisting of fibres with the same aspect ratio, A-B and C-D (Fig 21). Such a behaviour is the same as seen before for the networks with fibres of a varying fibre length (Fig 19). The form of the dependence of the degree of packing on the fibre aspect ratio agrees with that from the theory for maximum unforced packing.[5,20] When comparing the simulated results to theoretical considerations, we use the expression for the maximum unforced packing, (*Eq. 4*), with a caging number assumed to be 8 in Toll's work. The simulated resulting wet solid volume fraction shows very good agreement with the calculated maximum unforced packing.

The simulated average number of fibre-fibre contacts (Fig 21) has a relatively constant value for all four networks in the range of 7.5 – 9.4, which is similar to the simulations of the caging number and stability onset by Wouterse et al.[20] In that work, the authors obtain values of 9 and 7.5 for the average number of fibre-fibre contacts based on the Linear Complementarity Problem (LCP) and Molecular Dynamics (MD) simulations, respectively.

Based on the demonstrated very good agreement between the simulated results and the measurements from the unloaded network in Base Case (Fig 19), together with the conclusion that the simulated networks transition to a mechanically stable state within the narrow range of stability onset and maximum unforced packing (Fig 21), we are able to conclude that:

- The state to which pulp fibre networks are settling after the dry-to-wet transition in an unloaded case is a mechanically stable state within the narrow range of stability onset and maximum unforced packing.
- The level of the solid volume fraction to which the networks are tending after the dry-to-wet transition is determined primarily by the aspect ratio of the constituent fibres.

To conclude, these results again highlight the everchanging nature of this type of material. Transitioning from dry to wet state can drastically deform the material and the solid volume fraction no longer is dependent on fibre-fibre adhesion and historic pressure states but reverts to being predetermined by the fibre aspect ratio.

6. Summary and conclusions

The work in this thesis is based on combining experimental, numerical and theoretical approaches to advance our fundamental understanding of mechanical response and deformation in non-bonded anisotropic pulp fibre networks due to uniaxial compression, tensile stress and the spontaneous deformation due to the network transitioning from a dry to a wet state.

- In Paper I we show that for uniaxial compression the numerical framework replicates the established pressure vs solid volume fraction relationships as a power-law with a threshold solid volume fraction. We further explain the relationship between network deformation and deformation of the constituent fibres for this type of networks by showing that the response in a lower solid volume fraction range is dominated by the fibre bending deformation mode, while at relatively higher solid volume fraction, fibre-fibre contact deformation takes up a dominant role. This is in contrast to isotropic networks where the response in a lower solid volume fraction range is similarly dominated by the fibre bending deformation mode, while at relatively higher solid volume fraction, fibre axial deformation dominates.
- From the results in Paper II we have been able to explain the scaling of network strength with solid volume fraction and bond strength for low density anisotropic networks. For the scaling of elastic modulus the results showed the typical transition from bending to stretching fibre deformation being accompanied by changing values of the exponent, reconfirming literature result. The simulation results for both elastic modulus and strength showed excellent agreements with the respective experimental data in the literature.
- The results from Paper I and II highlight the important influence of unloaded network solid volume fraction on network response to both compressive and tensile deformation. For uniaxial compression the crucial impact of the unloaded solid volume fraction is seen by the dependence of pressure development on the threshold density, ρ_{th}. In tensile deformation the importance is seen by the number of bonded fibre-fibre contacts, directly dependent on the solid volume fraction, being a prime source of network strength. This leads to understanding of changes to the unloaded solid volume fraction of networks becoming paramount.
- In Paper III we have used simulated results to independently explain the effects of fibre rearrangement, fibre-fibre adhesion and elasto-plastic fibre-fibre contact deformation on changes in unloaded solid volume fraction due to uniaxial compression.
  We show that:
  - fibre rearrangement does not contribute to changes in the solid volume fraction for this type of networks.
  - adding inter-fibre adhesion has an effect on non-reversible deformation in the simulated networks. The impact of adhesion is, however, limited to a low-solid volume fraction range where the adhesive forces can overcome the fibre deformation forces and moments.
  - elasto-plastic nature of contacts between fibres introduces an effect on non-reversible deformation in the cases with large network strain where the yield criterion in the contact points is exceeded.
  - there is a clear synergetic effect of fibres having combined elasto-plastic contacts and adhesion where the included physical phenomena reinforce each other leading

to a degree of non-reversible deformation of the network far beyond that of networks with only elasto-plastic fibre contacts or inter-fibre adhesion.

Using experimental and numerical results we are able to show that the changes in unloaded solid volume fraction due to uniaxial compression in pulp fibre networks can be explained as dominated by fibre-fibre adhesion for low degrees of compression while for large network strain the non-reversible deformation being due to a synergetic effect of inter-fibre adhesion and fibre plastic deformation in the contact points.

- In the final paper we explain the change in pulp fibre networks due to transitioning from a dry to a wet state. From studying wetting of networks experimentally, numerically and theoretically we show that the state to which the network transitions when going from dry to wet is independent of its prior dry solid volume fraction. This infers that no fibre or network parameter that affects the wet solid volume fraction of the networks is affected by a prior dry compression or that the effect is annulled by the presence of water for the range of dry solid volume fractions studied. We further show that the change in the network solid volume fraction can be explained as driven by the disappearance of adhesion and that the mechanically stable state to which the network transitions is closely related to the theoretical maximum unforced packing and predetermined primarily by the fibre aspect ratios of the constituent fibres.

7. Reflections and outlook

Overall, the findings in this work and existing literature paint the picture of fluff pulp fibre networks as an ever-changing material where network stress, historic network stress or changes in contact mechanics between fibres often lead to drastically changing material behaviour in terms of mechanical response and fluid transport properties. The material is also expressing a wide range of regimes, with very varying responses to stresses. The prevalent regime depends on the network properties such as solid volume fraction, individual fibre properties in the form of aspect ratio, stiffness and fibre-fibre contact mechanics, as well as on the form of network stress.

The mechanical behaviour of the networks is very much a result of their nature, being a stack of elongated particles with weak or non-existent attractive forces between particles. The particle aspect of the network infers that the only way of force propagation through the network is through fibre-fibre contacts. The fact that networks consist of elongated flexible particles leads to that the number density of contacts can change drastically with changes in the solid volume fraction, leading to drastic changes in force propagation. This places great emphasis on understanding the number density of fibre-fibre contacts and the contact mechanics between fibres, making these two parameters perhaps the most important ones in order to understand macroscopic mechanical behaviour of the material.

The importance of fibre-fibre contact density and contact mechanics for macroscopic network behaviour introduces significant complexity when trying to understand and characterize networks experimentally. Fibre-fibre contact density is effectively impossible to measure accurately by any existing experimental procedure. A desirable approach would, for example, be some quick and convenient 3D visual method such as a CT-scan. However, the extreme resolution required to accurately identify a contact, in combination with the heterogeneity of the material requiring a large volume measured in order to have a representative measurement, renders this approach currently practically unviable. The sole comfort in this matter is the existence and practical usefulness of the relationship between the contact density and the network solid volume fraction derived from statistical geometry modelling. For fibre-fibre contact mechanics, single fibre measurements for compressive stiffness and attractive forces are possible and some results are indeed available in literature. However, measurements being on single fibres on a micro-level, in addition to the natural variation in fibres requiring large number of measurements in order to characterize fibres accurately, leads to a characterization of these parameters requiring a significant effort. Quick and simple methods for an accurate characterization of compressive and attractive fibre-fibre forces would thus be hugely beneficial for this field.

In light of the abovementioned, modelling of networks at an individua fibre level (such as with the DEM framework employed in this work) is of great value when understanding and characterizing network deformation and mechanical response. This is especially true regarding detection of fibre-fibre contacts, which is readily quantifiable from such modelling, thus providing in-depth information related to a parameter of crucial importance for network behaviour. Note that for contact mechanics, this type of modelling approach does not resolve the difficulties of accurately characterizing the complex contact mechanics of fibres, but rather enables us to control this parameter in ways unattainable by experimental means. The modelling allows for hypothesis testing of the physics involved and opens up ways for answering fundamental questions regarding deformation and network response as exemplified in e.g. Papers III and IV of this thesis. The main

strength of DEM, as opposed to other modelling approaches, is in handling the relative motion of particles and the emergence and disappearance of contact-points, which makes DEM the most effective for modelling conditions where these are dominating factors. This makes the numerical framework chosen in this thesis particularly useful for low solid volume fraction networks of non-bonded fibres or fibres with adhesive contacts. Given the complexity of simulation procedure and the involved computational costs, the usefulness of DEM lies primarily in the answering of fundamental questions rather than it being a tool for prediction of individual material behaviour.

8. Contribution statement

Paper I

I developed the code for pre-processing and post-processing of simulations. In cooperation with the main author, Shakhawath Hossain, we together did all implementation into the DEM solver and performed all simulations. I participated in the analysis together with my co-authors and contributed to the writing of the manuscript.

Paper II

I was the main author and developed the code for pre-processing and post-processing of simulations. In cooperation with a co-author, Shakhawath Hossain, we together did all implementation into the DEM solver and performed all simulations. I performed all analysis with support of the co-authors.

Paper III

I was the main author and, given the switch in DEM solver compared to the earlier work, developed the code for pre-processing, post-processing of simulations and performed all implementation into the DEM solver from scratch. I performed all analysis with support of the co-authors.

Paper IV

I was the main author and developed the code for pre-processing, post-processing of simulations, performed all implementation into the DEM solver and performed all simulations. I performed all analysis with support of the co-authors.

References

1. Picu R. Mechanics of random fiber networks—a review. *Soft Matter*. 2011;7(15):6768-6785.
2. Van Wyk C. 20—Note on the compressibility of wool. *Journal of the Textile Institute Transactions*. 1946;37(12):T285-T292.
3. Komori T, Makishima K. Numbers of fiber-to-fiber contacts in general fiber assemblies. *Textile Research Journal*. 1977;47(1):13-17.
4. Komori T, Itoh M. A modified theory of fiber contact in general fiber assemblies. *Textile research journal*. 1994;64(9):519-528.
5. Toll S. Packing mechanics of fiber reinforcements. *Polymer Engineering & Science*. 1998;38(8):1337-1350.
6. Toll S, Manson J-A. Elastic compression of a fiber network. 1995;
7. Rawal A. Microstructural insights into the enigmatic network of random fibers: van Wyk's notions revisited. *Computational Materials Science*. 2023;228:112307.
8. Evans K, Gibson A. Prediction of the maximum packing fraction achievable in randomly oriented short-fibre composites. *Composites Science and Technology*. 1986;25(2):149-162.
9. Rodney D, Fivel M, Dendievel R. Discrete modeling of the mechanics of entangled materials. *Physical review letters*. 2005;95(10):108004.
10. Subramanian G, Picu CR. Mechanics of three-dimensional, nonbonded random fiber networks. *Physical Review E*. 2011;83(5):056120.
11. Barbier C, Dendievel R, Rodney D. Role of friction in the mechanics of nonbonded fibrous materials. *Physical Review E*. 2009;80(1):016115.
12. Guo Y, Li Y, Liu Q, et al. An Investigation on triaxial compression of flexible fiber packings. *AIChE Journal*. 2020;66(6):e16946.
13. Guo Y, Li Y, Liu Q, et al. Discrete Element Method Model of Elastic Fiber Uniaxial Compression. *arXiv preprint arXiv:190902927*. 2019;
14. Guo Y, Wassgren C, Curtis JS, Xu D. A bonded sphero-cylinder model for the discrete element simulation of elasto-plastic fibers. *Chemical Engineering Science*. 2018;175:118-129.
15. Negi V, Picu R. Mechanical behavior of nonwoven non-crosslinked fibrous mats with adhesion and friction. *Soft matter*. 2019;15(29):5951-5964.
16. Negi V, Picu R. Mechanical behavior of cross-linked random fiber networks with inter-fiber adhesion. *Journal of the Mechanics and Physics of Solids*. 2019;122:418-434.
17. Ban E, Barocas VH, Shephard MS, Picu RC. Softening in random networks of non-identical beams. *Journal of the Mechanics and Physics of Solids*. 2016;87:38-50.
18. Head D, Levine A, MacKintosh F. Distinct regimes of elastic response and deformation modes of cross-linked cytoskeletal and semiflexible polymer networks. *Physical Review E*. 2003;68(6):061907.
19. Guo Y, Liu Q, Li Y, et al. Discrete element method models of elastic and elastoplastic fiber assemblies. *AIChE Journal*. 2021;67(8):e17296.
20. Wouterse A, Luding S, Philipse AP. On contact numbers in random rod packings. *Granular Matter*. 2009;11(3):169-177.
21. Grima A, Wypych P. Discrete element simulation of a conveyor impact-plate transfer: calibration, validation and scale-up. *Australian Bulk Handling Review*. 2010;3:64-72.
22. Zhou H, Chen Y, Sadek MA. Modelling of soil–seed contact using the Discrete Element Method (DEM). *Biosystems Engineering*. 2014;121:56-66.

23. Boac JM, Ambrose RK, Casada ME, Maghirang RG, Maier DE. Applications of discrete element method in modeling of grain postharvest operations. *Food Engineering Reviews*. 2014;6:128-149.
24. Van Lysebetten G, Vervoort A, Maertens J, Huybrechts N. Discrete element modeling for the study of the effect of soft inclusions on the behavior of soil mix material. *Computers and Geotechnics*. 2014;55:342-351.
25. Mahmoudi AH, Hoffmann F, Peters B. Application of XDEM as a novel approach to predict drying of a packed bed. *International Journal of Thermal Sciences*. 2014;75:65-75.
26. Picu R, Subramanian G. Correlated heterogeneous deformation of entangled fiber networks. *Physical Review E*. 2011;84(3):031904.
27. Abd El-Rahman A, Tucker III C. Mechanics of random discontinuous long-fiber thermoplastics. Part II: Direct simulation of uniaxial compression. *Journal of Rheology*. 2013;57(5):1463-1489.
28. Rigdahl M, Hollmark H. Network mechanics. *Paper Structure and Properties, Marcel Dekker, New York*. 1986:241-266.
29. Licup AJ, Sharma A, MacKintosh FC. Elastic regimes of subisostatic athermal fiber networks. *Physical Review E*. 2016;93(1):012407.
30. Eriksson M, Torgnysdotter A, Wågberg L. Surface modification of wood fibers using the polyelectrolyte multilayer technique: effects on fiber joint and paper strength properties. *Industrial & Engineering Chemistry Research*. 2006;45(15):5279-5286.
31. Gurnagul N, Seth R. Wet-web strength of hardwood kraft pulps. *Pulp & Paper Canada*. 1997;9:305-309.
32. Andersson SR. *Network Disruption and Turbulence in Fibre Suspensions*. Chalmers University of Technology; 1998.

Appendix I: Governing equations

Translational and rotational motion of a particle	$m_i \ddot{\boldsymbol{r}}_i = \sum_j \boldsymbol{F}_{ij} + \boldsymbol{F}_i^B$ $\boldsymbol{I}_i \ddot{\boldsymbol{\theta}}_\iota = \sum_j \boldsymbol{T}_{ij}$	Here m_i is the mass and $\ddot{\boldsymbol{r}}_i$ is the acceleration of the i-th particle, $\boldsymbol{F}_{ij}$ is the interaction force between the i-th and j-th particle and $\boldsymbol{F}_i^B$ is the body force acting on the i-th particle. For the angular momentum, $\boldsymbol{I}_i$ is the moment of inertia tensor, $\ddot{\boldsymbol{\theta}}_\iota$ is the angular acceleration and $\boldsymbol{T}_{ij}$ is the interaction torque between the i-th and j-th particle. Interaction forces and moments are different for bonded and non-bonded particles. Non-bonded particles can interact by normal and tangential contact forces, $\boldsymbol{F}_{ij}^c$, and moments, $\boldsymbol{T}_{ij}^c$ arising from contact forces. For bonded particles the contact interaction is disabled and the interaction forces, $\boldsymbol{F}_{ij}^b$, and moments, $\boldsymbol{T}_{ij}^b$, come from the bonded interaction.
Contact interaction	$\boldsymbol{F}_{ij} = \boldsymbol{F}_{ij}^c$ $F_n^c = \frac{4}{3} E_c \sqrt{R} \delta_n^{3/2}$ $F_t^c = 8 G_c \sqrt{R} \delta_n^{3/2}$	Here E_c is the contact Young's modulus, G_c is the contact shear modulus, R is the particle radius and δ_n is the normal overlap. δ_n is the tangential displacement between the particles during the time they are in contact and truncated to fulfil $F_t^c \leq \mu F_n^c$.
Bonded interaction	$\boldsymbol{F}_{ij} = \boldsymbol{F}_{ij}^b$ $\boldsymbol{T}_{ij} = \boldsymbol{T}_{ij}^b$ $F_n^b = \frac{E_b A}{l_b} \delta_n^b$ $F_t^b = \frac{G_b A}{l_b} \delta_t^b$ $dT_n^b = \frac{G_b I}{l_b} d\theta_n^b$ $dT_t^b = \frac{E_b I}{l_b} d\theta_t^b$	Here E_b is the bond Young's modulus, G_b is the bond shear modulus, δ^b is the bond displacement from equilibrium distance and θ^b is the bond angle.
Body forces	$\boldsymbol{F}_i^B = m_i \boldsymbol{g} - \gamma \dot{\boldsymbol{r}}_i$	Here $\boldsymbol{g}$ is the gravity vector, $\dot{\boldsymbol{r}}_i$ is the velocity vector and γ is a damping coefficient.

Typical input parameters for DEM simulations

Fibre properties	**Value**
Particle diameter, D [μm]	18
Length of a bond, l_b [μm]	18
Particle density, ρ_p [kg/m^3]	1000
Particle contact elastic modulus, E_c [GPa]	1.0
Bond bending modulus, E_b [GPa]	4.0
Particle Poisson's ratio [-]	0.3
Particle-particle friction coefficient [-]	0.3
Particle-wall friction coefficient [-]	0.3
Wall contact elastic modulus, E_w [GPa]	10
Time step size [s]	$2 \cdot 10^{-9}$